Title page

Dynamics and Regulatory Roles of RNA m^{6}A Methylation in Unbalanced Genomes

Shuai Zhang,[1,2,†] Ruixue Wang,[1,2,†] Kun Luo,[1,2] Shipeng Gu,[1,2] Xinyu Liu,[1,2,] Junhan Wang,[1,2] Ludan Zhang,[1,2] and Lin Sun[1,2,*]

[1] Key Laboratory of Cell Proliferation and Regulation Biology of Ministry of Education, College of Life Sciences, Beijing Normal University, Beijing 100875, China

[2] Beijing Key Laboratory of Gene Resource and Molecular Development, College of Life Sciences, Beijing Normal University, Beijing 100875, China

† These authors contributed equally to this work.

* For correspondence: sunlin@bnu.edu.cn (Lin Sun)

Abstract

N^6-methyladenosine (m^{6}A) in eukaryotic RNA is an epigenetic modification that is critical for RNA metabolism, gene expression regulation, and the development of organisms. Aberrant expression of m^{6}A components appears in a variety of human diseases. RNA m^{6}A modification in *Drosophila* has proven to be involved in sex determination regulated by *Sxl* and may affect X chromosome expression through the MSL complex. The dosage-related effects under the condition of genomic imbalance (i.e., aneuploidy) are related to various epigenetic regulatory mechanisms. Here, we investigated the roles of RNA m^{6}A modification in unbalanced genomes using aneuploid *Drosophila*. The results showed that the expression of m^{6}A components changed significantly under genomic imbalance, and affected the abundance and genome-wide distribution of m^{6}A, which may be related to the developmental abnormalities of aneuploids. The relationships between methylation status and classical dosage effect, dosage compensation, and inverse dosage effect were also studied. In addition, we demonstrated that RNA m^{6}A methylation may

affect dosage-dependent gene regulation through dosage-sensitive modifiers, alternative splicing, the MSL complex, and other processes. More interestingly, there seems to be a closely relationship between MSL complex and RNA m^6A modification. It is found that ectopically overexpressed MSL complex, especially the levels of H4K16Ac through MOF could influence the expression levels of m^6A modification and genomic imbalance may be involved in this interaction. We found that m^6A could affect the levels of H4K16Ac through MOF, a component of the MSL complex, and that genomic imbalance may be involved in this interaction. Altogether, our work reveals the dynamic and regulatory role of RNA m^6A modification in unbalanced genomes, and may shed new light on the mechanisms of aneuploidy-related developmental abnormalities and diseases.

Introduction

Epigenetic modifications regulate gene expression in response to environmental changes and play important roles in the development of organisms and a variety of human diseases (Jaenisch and Bird, 2003; Lence et al., 2017). In addition to DNA and chromatin modifications, which are well studied, more than one hundred RNA chemical modifications have been identified in cells to date (Lee et al., 2014; Roundtree et al., 2017a). As a marker of post-transcriptional regulation, RNA modifications participate in almost all aspects of RNA metabolism (Roundtree et al., 2017a). N^6-methyladenosine (m^6A) is the most prevalent internal modification in many eukaryotic messenger RNAs (mRNAs) and long noncoding RNAs (lncRNAs) (Lee et al., 2014; Roundtree et al., 2017a; Yang et al., 2018), which widely affects RNA alternative splicing (Dominissini et al., 2012), export (Roundtree et al., 2017b), stability (Wang X et al., 2014), and translation (Meyer et al., 2015). RNA m^6A modifications have been found to be enriched on the transcripts of genes that regulate development and cell fate specification (Dominissini et al., 2012; Meyer et al., 2012; Geula et al., 2015), and some m^6A sites are regulated in a tissue- or disease-specific manner (Zaccara et al., 2019). In addition, the abnormal expression of m^6A components is related to the tumorigenesis, proliferation, and metastasis of many types of cancers (Pinello et al., 2018; Ma et al., 2019). Therefore, it is of great significance to study RNA m^6A methylation for revealing the

57 mechanisms of gene expression regulation and human diseases.

58 At present, there are few studies on RNA m^6A modification in *Drosophila*, possibly due to its
59 relatively low abundance ($m^6A/A < 0.2\%$) (Haussmann et al., 2016), and the mutation of some
60 m^6A component genes will affect their viability and fertility (Hongay and Orr-Weaver, 2011;
61 Haussmann et al., 2016; Kan et al., 2017). However, as a model organism with specific genetic
62 and developmental advantages, *Drosophila* remains an excellent tool for studying the roles of
63 epigenetic modifications in gene regulation, individual development, and disease process. Several
64 components of the *Drosophila* m^6A methyltransferase complex (*Ime4*, *dMettl14*, and *fl(2)d*
65 constitute the core complex, with *vir* and *nito* acting as cofactors) and a m^6A reader protein
66 (*Ythdc1*) have been identified, all of which have homologues in mammals (Lence et al., 2017).
67 Deletion of the major methyltransferase gene *Ime4* or the reader *Ythdc1* causes locomotion
68 defects, and the splicing of sex-determining factor *Sxl* is affected (Haussmann et al., 2016; Lence
69 et al., 2016; Kan et al., 2017). However, homozygous mutations in *fl(2)d*, *vir*, and *nito* were lethal,
70 suggesting that these subunits have important functions other than methylation (Penn et al.,
71 2008; Yan et al., 2015; Kan et al., 2017; Lence et al., 2017). RNA m^6A modification has an obvious
72 sexual dimorphism in *Drosophila*, and reduced m^6A levels severely decreased the survival of
73 females. It is thought to be due to the derepression of *msl-2* caused by aberrantly spliced *Sxl*,
74 which forms the Male Specific Lethal (MSL) complex that associates with the X chromosome
75 (Haussmann et al., 2016).

76 Dosage compensation is a widespread phenomenon in unbalanced genomes (Lucchesi, 2018;
77 Birchler and Veitia, 2021). The deletion or duplication of some chromosomes rather than the
78 whole chromosome set leads to genomic imbalance, that is, aneuploidy (Orr et al., 2015).
79 Aneuploid variation is usually detrimental to organisms (Birchler and Veitia, 2012; Orr et al., 2015;
80 Birchler and Veitia, 2021), and is associated with developmental abnormalities, mental
81 retardation, and various congenital defects (Williams et al., 2008; Huang et al., 2021;
82 Sanchez-Pavon et al., 2021), possibly due to disorders in their gene expression systems (Prestel et
83 al., 2010; Letourneau et al., 2014). Studies across species have pointed out that there is
84 genome-wide *trans* modulation in aneuploidy, and the genes on the varied chromosomes are
85 compensated to a certain extent, while genes located on the rest of the genome are mainly
86 regulated in the opposite direction to the changes of chromosome numbers, which is known as

87 the inverse dosage effect (Birchler and Veitia, 2012, 2021; Sun et al., 2013c; Hou et al., 2018; Shi
88 et al., 2021). Histone modification (Zhang et al., 2021a), chromatin remodeling (Birchler, 2016),
89 lncRNAs (Zhang et al., 2023) and microRNAs (Shi et al., 2022) have all been shown to play a role
90 in genomic imbalance.

91 Because of the haploinsufficiency for X-linked genes, heterogametic individuals in organisms
92 with XY sex determination systems could be regarded as analogous to aneuploidy (Disteche,
93 2016), including humans and *Drosophila*. Some studies have linked histone H4 lysine 16
94 acetylation (H4K16Ac) and non-coding *roX* RNAs to the dosage compensation of *Drosophila* (Park
95 et al., 2010; Conrad et al., 2012). On the other hand, the compensation of X chromosome in
96 human is thought to be regulated by lncRNA X-inactive specific transcript (*XIST*) (Jordan et al.,
97 2019). Interestingly, in *Drosophila*, RNA m^6A modification indirectly affects gene expression
98 through *Sxl* and *msl-2*; while in human, m^6A methylation of the key lncRNA *XIST* is necessary for
99 the silencing of gene transcription on one of the female X chromosomes (Patil et al., 2016).
100 Moreover, most tumor cells have genomic instability and high levels of aneuploidy (Ben-David
101 and Amon, 2020; Chiarle, 2021), and at the same time, m^6A component genes are often
102 aberrantly expressed in various cancers (Pinello et al., 2018; Ma et al., 2019).

103 An increasing number of studies have found that dosage-related effects in aneuploidy may be
104 the integration of multiple modulations rather than through a single mechanism (Prestel et al.,
105 2010; Birchler, 2016). The effects of genomic imbalance are complicated, and the model of
106 dosage compensation and global gene regulation in *Drosophila* has been extended to autosomal
107 aneuploidies and sex chromosome aneuploid metafemales where MSL complexes are not
108 assembled (Sun et al., 2013b,c; Zhang et al., 2021b). In addition, genomic imbalance and *trans*
109 regulatory mechanisms in other species such as maize, *Arabidopsis*, and humans have also been
110 investigated (Hou et al., 2018; Raznahan et al., 2018; Shi et al., 2021; Yang et al., 2021; San
111 Roman et al., 2023). To reveal the role of RNA m^6A modification in unbalanced genomes, we
112 studied the dynamic changes and regulatory functions of m^6A methylation under genetic
113 imbalance conditions using autosomal and sex chromosome aneuploid *Drosophila* maintained in
114 our laboratory. Meanwhile, dosage-sensitive modifiers, differential alternative splicing events,
115 the MSL complex and other factors that may mediate the relationships between RNA m^6A
116 modification and the dosage-related effects of aneuploidy were also investigated. In summary,

117 we provided a comprehensive picture of RNA m^6A methylation in unbalanced genomes.

118

119

120 # Results

121 ## The responses of m^6A components under genomic imbalance

122 RNA m^6A methylation is a reversible epigenetic modification, and its dynamic process is mediated
123 by m^6A methyltransferases (writers), demethylases (erasers), and m^6A recognition proteins
124 (readers) (Lee et al., 2014; Yang et al., 2018; Zaccara et al., 2019) (Figure 1A). We first detected
125 the expression of m^6A components in *Drosophila* larvae with karyotypes of normal diploids and
126 trisomies that have an additional chromosome arm using RT-qPCR to determine whether RNA
127 m^6A dynamics are affected by correlative enzymes in unbalanced genomes (Figure 1B; Figure
128 1—figure supplement 1A,B). It was found that the transcription levels of most m^6A writers and
129 the major m^6A reader are down-regulated in aneuploids compared with their respective
130 sex-corresponding controls (Figure 1B). Unlike the other components, the cofactor *vir* of
131 methyltransferase complex is up-regulated in trisomy 2L females (Haussmann et al., 2016; Lence
132 et al., 2016; Kan et al., 2017). Because RNA m^6A modification is enriched in the nervous system of
133 *Drosophila*, the brains of aneuploid third instar larvae were also used to detect the expression of
134 m^6A components. As expected, a decreased expression trend of m^6A components similar to that
135 of the whole larvae was observed (Figure 1—figure supplement 1C).

136 Previous studies have pointed out that the m^6A methylomes have temporal and spatial
137 specificity in the development process of organisms, especially for embryonic development and
138 cell differentiation (Meyer and Jaffrey, 2014; Wang Y et al., 2014). Aberrant expression of m^6A
139 components may cause defects in embryogenesis and even early embryonic lethality (Zhong et
140 al., 2008; Wang Y et al., 2014; Geula et al., 2015; Zhao et al., 2017). Therefore, we designed
141 probes of m^6A components (Figure 1—figure supplement 1D,E) to examine the mRNA expression
142 and localization patterns during early embryonic development of aneuploid *Drosophila* using
143 high-resolution TSA-FISH (Lecuyer et al., 2007; Jandura et al., 2017). The results showed that the
144 subembryonic distribution patterns of the five components of m^6A methyltransferase complex

145 and one m^6A reading protein are similar in wildtype and aneuploidies (Figure 1C,D; Figure
146 1—figure supplement 2A-F). At the blastoderm stage (stage 1-5), the probe signals of m^6A
147 components are widely distributed in the surface cell layer, yolk plasma, yolk cortex, and show a
148 pattern of basal enrichment (Figure 1—figure supplement 2A-F). For the gastrulae at stage 6-11,
149 the transcripts of m^6A components are mainly located in head, amnioproctodeal invagination,
150 germ band, and as in previous studies (Lence et al., 2016), and show an enrichment in
151 neuroectoderm (Figure 1C; Figure 1—figure supplement 2A-F). At later stages of embryonic
152 development (stages 12-13 and 14-17), the probes are distributed in brain, ventral nerve cord,
153 midgut, and salivary gland (Figure 1C; Figure 1—figure supplement 2A-F).

154 By observing the subcellular localization of the probe signals of m^6A components at higher
155 magnification, it can be found that most of the mRNAs of these genes have nuclei-associated
156 localization patterns (Figure 1D; Figure 1—figure supplement 2A'-F'). In the early and late stages
157 of embryonic development, the probe signals of *Ime4*, *dMettl14*, *fl(2)d*, *vir*, and *Ythdc1* form
158 dense small foci near the nucleus, which is a perinuclear distribution (Figure 1D; Figure 1—figure
159 supplement 2A'-F'). For *nito*, in addition to the perinuclear signals, there is also an obvious signal
160 of intranuclear localization during early embryogenesis, which is manifested as one or two small
161 foci in the blastoderm nucleus (Figure 1D; Figure 1—figure supplement 2E').

162 Although there seems to be no difference in the localization of the transcripts of m^6A
163 components that we detected in aneuploidy and wildtype embryos, the expression levels of
164 these genes, as determined by relative fluorescence intensity, are significantly changed (Figure
165 1E,F; Figure 1—figure supplement 2A"-F"). Except for the irregular fluctuations at early
166 embryonic stages, the expression levels of most m^6A components in aneuploids are lower than
167 those in wildtype at more mature stages (Figure 1E,F; Figure 1—figure supplement 2A"-F"), which
168 is similar to the trend we detected in third instar larvae (Figure 1B; Figure 1—figure supplement
169 1C). The transcripts of m^6A methyltransferase and reader protein have specific subembryonic and
170 subcellular localization patterns in the development of *Drosophila* embryos, which may be a
171 mechanism to regulate cellular functions, and ensure appropriate cell growth and differentiation
172 (Lecuyer et al., 2007).

173

174 **Genome-wide mapping of RNA m^{6}A methylation in aneuploid *Drosophila***

175 Subsequently, we detected the global levels of RNA m^{6}A methylation in wildtype and aneuploid
176 *Drosophila* larvae to determine whether m^{6}A abundance is altered under the condition of
177 genomic imbalance due to modulation by transmethylases. The overall abundance of m6A was
178 represented by the m^{6}A/A ratio in total RNA (Figure 2A). It was found that the m^{6}A abundance of
179 wildtype males is higher than that of females, but both are lower than 0.2%, which is consistent
180 with the finding that m^{6}A levels in *Drosophila* are relatively low (Haussmann et al., 2016; Lence et
181 al., 2016). Females with triple chromosome 2 left arms (2L) and metafemales with triple X
182 chromosomes have significantly higher m^{6}A abundances than diploid females, whereas there is
183 no significant difference between trisomy 2L males and wildtype males (Figure 2A). Therefore,
184 genomic imbalance can affect the m^{6}A methylation status to some extent, and this epigenetic
185 modification is different between males and females. However, the m^{6}A abundance in
186 aneuploidies did not follow the expression levels of transmethylases.

187 To obtain m^{6}A mapping across the transcriptome of aneuploid *Drosophila*, whole larvae with
188 different karyotypes were used for m^{6}A methylated RNA immunoprecipitation sequencing
189 (MeRIP-Seq). By identifying consistent peaks in two biological replicates, approximately ten
190 thousand m^{6}A peaks were found in wildtype females and males, whereas there were less than
191 half the number of methylation sites in the three kinds of aneuploidies (Figure 2B). When these
192 m^{6}A sites were annotated to the genes, the changes in the number of m^{6}A-marked genes in
193 samples of different genotypes were in accordance with that of m^{6}A peaks, in which there are
194 about 2,500 m^{6}A-marked genes in wildtype and about 1,000 m^{6}A-modified genes in trisomies
195 (Figure 2C). Both the number of m^{6}A peaks and the number of m^{6}A-modified genes are the least
196 in trisomy 2L females (Figure 2B,C). The changes in the number of RNA methylation sites in
197 aneuploids did not coincide with the changes of overall m^{6}A abundance, but instead matched the
198 expression of m^{6}A components. We speculate that this may be caused by the nonuniformity and
199 heterogeneity of RNA m^{6}A modification, including the tissue specificity, the developmental
200 specificity, the different numbers of m^{6}A sites in one transcript, the different proportions of
201 methylated transcripts, et cetera (Meyer et al., 2012; Meyer and Jaffrey, 2014; Zaccara et al.,
202 2019). Counting the number of reads that mapped to m^{6}A peaks in wildtype and aneuploidy

203 MeRIP samples showed that the read levels at m^6A sites in aneuploidies are significantly higher
204 than that in wildtypes (Mann Whitney U test p-values < 0.001; Figure 2D); further analysis of the
205 relative IP/Input ratios showed that the values of aneuploidies are still higher than wildtypes
206 (Mann Whitney U test p-values < 0.001), which confirmed our hypothesis. These results suggest
207 that RNA m^6A modification exhibits greater heterogeneity in unbalanced genomes.

208 We next studied the overall characteristics of m^6A methylation in aneuploid and control
209 *Drosophila*. m^6A peaks are localized along all autosomes and sex chromosomes, and the numbers
210 of peaks are correlated with chromosome length (Figure 2—figure supplement 1A). Methylation
211 sites are widely distributed on 5'UTR (30-50%), 3'UTR (10-15%), promoter (15-20%), and internal
212 exons (20-35%), and the aneuploidies appeared to have a higher proportion of 5'UTR peaks and a
213 lower proportion of exon peaks than the wildtype (Figure 2E). The highest values of density
214 distributions of the length of exons containing m^6A peaks are around 250 bp, and approximately
215 90% of the exons are longer than the typical 140 bp (Figure 2—figure supplement 1B). *De novo*
216 motif analysis of m^6A methylation peaks in each sample showed that the top-ranked motif is
217 consistent with the conserved m^6A motif DRACH (D=G/A/U, R=G/A, H=U/A/C; Figure 2F). In
218 addition, enrichment analysis of the known motif DRACH showed that it is significantly enriched
219 in all samples, and more than 97% of the m^6A sites have this sequence (Figure 2—figure
220 supplement 1C).

221 There are 370 common genes to which the m^6A peaks were annotated in all genotypes
222 (Figure 2G). We classified the m^6A-modified genes in each sample and found that they were
223 mostly protein-coding genes, whereas only about 7% were ncRNAs (Figure 2H). As described in
224 previous studies (Meyer et al., 2012; Zaccara et al., 2019), most methylated RNAs have one m^6A
225 peak (Figure 2—figure supplement 1D-H). However, there are still some genes whose transcripts
226 can be highly methylated and contain more than five m^6A sites (Figure 2—figure supplement
227 1D-I). It was found that transcription factors were significantly enriched in 70 genes with more
228 than 5 m^6A peaks in both wildtype and aneuploidy (Fisher's exact test p-value = 7.7e-4; Figure 2I;
229 Figure 2—figure supplement 1I). Thus, specific types of genes may be preferentially targeted by
230 m^6A modification, such as transcriptional regulators (Kan et al., 2017). Analysis of the functions of
231 m^6A-modified genes in each sample revealed that they were enriched for a large number of
232 common functions, among which the most significant were those related to morphogenesis,

233 development, and growth (Figure 2—figure supplement 2A). The 141 GO terms shared by the
234 five genotypes were summarized and found to include functions about metabolism, regulation,
235 cellular processes, signaling pathways, behavior, and immune response (Figure 2—figure
236 supplement 2B,C). Through pathway enrichment analysis of m^6A-modified genes, 9 terms were
237 found to be consistently enriched in all samples, including MAPK signaling pathway, Hippo
238 signaling pathway, TGF-β pathway, etc. (Figure 2—figure supplement 2D-F).
239

240 **Differentially methylated peaks (DMPs) and their associated genes**

241 We then searched for the differential methylation peaks (DMPs) in autosomal and sex
242 chromosome aneuploidies compared with wildtype *Drosophila* of their corresponding sex. The
243 number of DMPs and the changing trend of DMP methylation status are shown in the Figures
244 (Figure 3A-D). In trisomy 2L females, the number of upregulated DMPs (1,131) is less than that of
245 downregulated DMPs (1,602). In trisomy 2L males, the number of upregulated DMPs (1,521) is
246 slightly higher than that of downregulated DMPs (1,259). In metafemales, the number of
247 upregulated DMPs (1,393) is higher than that of downregulated DMPs (926) (Figure 3A-D). More
248 DMP-associated genes were found in autosomal aneuploidies than in sex chromosome
249 aneuploidy (trisomy 2L female = 2,148, trisomy 2L male = 2,055, metafemale = 1,771; Figure 3E).
250 Also, the total number of peaks after the differential analysis would be different from the number
251 of m^6A peaks identified in the previous section, because the analysis software merged and
252 recalculated the peaks (Stark and Brown, 2013).
253 DMPs are distributed on all chromosomes (Figure 3—figure supplement 1A). Specifically, the
254 MeRIP-Seq signal intensity at the location of DMPs showed that the m^6A-marked reads in
255 trisomies are denser than those of wildtypes, especially on the triple chromosomes (Figure 3F-H).
256 The density of reads on chromosome 2L of trisomy 2L *Drosophila* is higher than that on other
257 chromosomes, while the density of reads on chromosome X of metafemales is significantly higher
258 than that of autosomes (Figure 3F-H). Previous studies on aneuploid *Drosophila* showed that the
259 expression levels of genes on chromosomes with increased copy numbers were mostly similar to
260 those in diploids, and the expression of genes on unvaried chromosomes were widely inverse
261 regulated (Sun et al., 2013c; Birchler, 2016; Zhang et al., 2023). It can be concluded that the

262 changes in the density of reads at DMP sites are not due to a direct gene dosage effect. Similar
263 results were obtained by counting the methylation status of cis and trans transcripts (Figure 3I-K).
264 Overall, the transcripts of genes located on the varied chromosomes in three trisomies have
265 more up-regulated DMPs than down-regulated DMPs, which is more obvious in metafemales
266 (Figure 3I-K). In trisomy 2L females and males, genes localized on other autosomes have a higher
267 proportion of down-regulated DMPs, while the X-linked *trans* genes show sexual dimorphism and
268 X chromosome-specific response to genomic imbalance. (Figure 3I,J). For metafemales, the
269 transcripts of *trans* genes have similar numbers of up-regulated and down-regulated DMPs
270 (Figure 3K). Therefore, *cis* genes in trisomy generally possessed a higher proportion of
271 up-regulated DMP-associated transcripts, whereas the methylation states of *trans* genes are
272 variable, depending on the identities of varied chromosomes and their genomic locations. The
273 above results give us reason to speculate that the changes of m^6A methylation may affect dosage
274 compensation of *cis*-genes and inverse dosage modulation of *trans*-genes in aneuploidy.

275 The distribution of DMPs along gene features includes 5'UTR (30-35%), 3'UTR (20-25%),
276 promoter (10-25%), and internal exon (25-35%), among which the proportion of 3'UTR is higher
277 than that of all m^6A sites (Figure 3—figure supplement 1B). The length distributions of exons with
278 DMPs are similar to that of all m^6A-modified exons (Figure 3—figure supplement 1C). *De novo*
279 motif analysis of the sequences where DMPs are located or enrichment analysis of the known
280 motif DRACH both showed that DMP sites are enriched for the conserved motif of m^6A (Figure
281 3—figure supplement 1D,E). There are also similarities between the types of DMPs-associated
282 genes and m^6A-marked genes (Figure 3—figure supplement 1F). The DMP-associated genes of
283 the three aneuploidies have complex overlapping relationships (Figure 3—figure supplement 1G).
284 Most DMP-associated genes have one differentially methylated site, and only a few genes
285 contained more than three DMPs (Figure 3—figure supplement 1H-J). There are 1,042 common
286 DMP-associated genes in all trisomies, of which 71 were transcription factors and were
287 significantly enriched (Fisher's exact test p-value = 6.9e-5; Figure 4A,B). We speculate that these
288 differentially methylated transcription factors may play an important role in the regulation of
289 gene expression and development of aneuploidy.

290 Functional enrichment analysis showed that genes with up-regulated DMPs in three trisomies
291 were enriched for 153 common functions, while the genes with down-regulated DMPs shared

292 only 6 functions (Figure 4—figure supplement 1A,B). Similarly, genes with up-regulated DMPs
293 were enriched for more consistent pathways in all aneuploids (Figure 4—figure supplement 1C,D).
294 Most of the functions of DMP-associated genes are the same as those of m^6A-marked genes, and
295 these genes are also enriched for cell fate commitment, dorsal/ventral pattern formation, sex
296 differentiation, post-transcriptional regulation of gene expression, and other additional GO terms.
297 We found that many DMP-associated genes have functions related to gene expression regulation
298 and dosage compensation, including some components of MSL complex (*msl-1*, *msl-3*,
299 *lncRNA:roX1*) and the major sex-determining factor *Sxl* (Figure 4C). We also noticed that m^6A
300 component genes *fl(2)d*, *nito*, and *Ythdc1* themselves are differentially methylated in aneuploidy
301 (Figure 4C), for example, there was a common significantly upregulated m^6A peak in the 5'UTR of
302 the transcripts of *fl(2)d* in three aneuploidies (Figure 4D). These data suggest that m^6A dynamics
303 in aneuploids may be involved in the expression regulation of unbalanced genomes through
304 various genes with regulatory functions.
305

306 **Relationships between m^6A and dosage-related modulation of gene expression in**
307 **aneuploidy**

308 To explore the relationships between RNA m^6A modification and gene expression regulation
309 under genomic imbalance, we combined the results of MeRIP-Seq and RNA-seq, and performed a
310 comprehensive analysis. The results showed that about 12%-15% of genes differentially
311 expressed in aneuploid *Drosophila* also belong to DMPs-associated genes (Figure 5A-C). However,
312 except for trisomy 2L males, the DEGs of the other two trisomies did not show enrichment of
313 differential m^6A methylation (Fisher's exact test p-values: trisomy 2L male = 0.012, trisomy 2L
314 female and metafemale > 0.05). There are 55 genes that are both differentially expressed and
315 differentially methylated in all aneuploidies (Figure 5D). By analyzing the functions of genes that
316 are simultaneously differentially expressed and differentially methylated, we obtained a number
317 of consistent biological functions, including post-embryonic animal morphogenesis, cell
318 communication, signal transduction, response to stimulation, and so on (Figure 5E), possibly
319 reflecting the important roles of m^6A-regulated expression in cell signaling and development of
320 organisms.

321 By analyzing the crossover of different groups of m^6A-modified genes and genes with
322 canonical dosage effect, dosage compensation, and inverse dosage effect, we further revealed
323 the relationships between m^6A-modified genes and dosage-related effects in aneuploidy (Figure
324 5F-H). The results showed that in trisomy 2L females, *cis* dosage compensation genes, *trans*
325 autosomal dosage effect genes, and *trans* unchanged genes are significantly enriched in m^6A
326 group with methylation in both trisomy and control; meanwhile, *cis* dosage effect genes, other
327 autosomal dosage effect genes, and X-linked dosage effect genes are enriched in the group
328 without methylation in both trisomy and control (Figure 5F). On the contrary, in trisomy 2L males,
329 *cis* dosage effect genes, *trans* dosage effect genes, and *trans* unchanged genes are significantly
330 enriched in m^6A group whose genes are methylated in both trisomy and control; while the group
331 of genes that are not methylated at all is enriched for *cis* dosage effect genes, *cis* dosage
332 compensation genes, *trans* inverse dosage effect genes, and other autosomal dosage effect genes
333 (Figure 5G). Metafemales performed similarly to trisomy 2L female, with significant enrichment
334 of *cis* dosage compensation genes, autosomal *trans* dosage effect genes, and *trans* unchanged
335 genes in m^6A group where both trisomy and control genes are methylated; and the group
336 without methylation is enriched for *cis* dosage effect genes and *trans* dosage effect genes (Figure
337 5H). These results indicated that m^6A-modified genes in aneuploid *Drosophila* females are mainly
338 related to dosage compensation and inverse dosage effect, while genes not modified by m^6A are
339 mainly related to direct dosage effect. Male aneuploids did not follow this trend.

340 Furthermore, the distributions of m^6A modification sites along gene features in genes with
341 classical dosage-related effects were also studied (Figure 5I-K). We found that in wildtype females,
342 trisomy 2L females, and metafemales, a higher proportion of m^6A sites on genes with canonical
343 dosage compensation and inverse dosage effect are distributed in the 5'UTR than genes with
344 dosage effects (Figure 5I,K). At the same time, this proportion is higher in trisomy than in
345 wildtype. In contrast to females, trisomy 2L males have a higher proportion of 5'UTR RNA m^6A
346 modification on dosage effect genes (Figure 5J). The above study again demonstrates the sexual
347 dimorphism of RNA m^6A modification in response to aneuploidy. In addition, it has been
348 suggested that m^6A residues in the 5'UTR region may have unique regulatory functions (Luo et al.,
349 2014; Meyer and Jaffrey, 2014). Therefore, we hypothesized that the high level of 5'UTR m^6A
350 modification on genes with dosage compensation and inverse dosage effect might regulate the

351 down-regulation of these genes.

352 Dozens of dosage-sensitive modifiers have been identified in *Drosophila*, whose dosage
353 changes can negatively or positively regulate the gene expression across the whole genome like
354 aneuploidy (Birchler et al., 2001; Birchler and Veitia, 2007). Protein-protein interaction (PPI)
355 networks between dosage-sensitive modifiers and differentially expressed genes (DEGs) were
356 constructed to investigate whether RNA m^6A modification could participate in the gene
357 regulatory networks in unbalanced genomes through these regulators (Figure 5—figure
358 supplement 1A-C). In the three types of aneuploidies, there are more dosage-sensitive modifiers
359 with up-regulated DMPs than with down-regulated DMPs. The regulators *ox* and *Vha55* without
360 DMPs interact with a large number of significantly up-regulated DEGs in trisomy 2L females and
361 metafemales, whereas these two regulators interact with a small number of down-regulated
362 DEGs in trisomy 2L males. Up-regulated DMP-associated regulators *wg*, *Uba1*, *ap*, *Atg1*, *osa*, *rdx*,
363 and *sd* in trisomy 2L females mainly interacted with significantly down-regulated DEGs (Figure
364 5—figure supplement 1A); and up-regulated DMP-associated regulators *Uba1*, *osa*, and *sd* in
365 metafemales also interacted with down-regulated DEGs (Figure 5—figure supplement 1C).
366 Up-regulated DMP-associated regulators *wg*, *Kr-h1*, and *Trl* mainly interacted with up-regulated
367 DEGs in trisomy 2L males (Figure 5—figure supplement 1B). In addition, a preponderance of
368 significantly down-regulated DEGs interacted with dosage-sensitive modifiers is observed on
369 *trans* chromosomes of all *Drosophila* trisomies (Figure 5—figure supplement 1A-C).

370

371 Alterations of m^6A may be involved in differential alternative splicing in imbalanced 372 genomes

373 Next, we analyzed the differential alternative splicing events in aneuploid *Drosophila*. More than
374 1,000 differential splicing events have been identified in different aneuploids, and about
375 one-third of them are of the type of skipped exon (SE) (Figure 6—figure supplement 1A-C). The
376 biological functions of differentially spliced transcripts are mainly involved in macromolecular
377 fiber organization, locomotion, and growth (Figure 6—figure supplement 1D), and these genes
378 are enriched in heterogeneous pathways in different aneuploidies (Figure 6—figure supplement
379 1E). Notably, we found that genes with DMPs are significantly enriched for differential alternative

380 splicing events in three kinds of aneuploid *Drosophila* (Fisher's exact test p-values < 0.05; Figure
381 6A-C). Among the genes whose transcripts are differentially spliced, 27%-32% are also
382 differentially methylated (Figure 6A-C). There are 67 genes with both differential alternative
383 splicing and differential m^6A methylation in all aneuploidies (Figure 6D). The functions of these
384 genes are similar to those of all differentially spliced genes (Figure 6E), but more consistent KEGG
385 pathways are enriched, including endocytosis, mTOR signaling pathway, Hedgehog signaling
386 pathway, and so on (Figure 6F).

387 In all trisomy *Drosophila*, 10 genes are shown to be differentially expressed, with their
388 transcripts also being differentially spliced and differentially methylated. Three of them are
389 illustrated below [*su(Hw)*, *Ppn*, and *CG13124*]. *su(Hw)* is a component of the gypsy chromatin
390 insulator complex, which is a regulatory element that establish independent domains of
391 transcriptional activity (Roseman et al., 1993). Due to the close relationship between *su(Hw)* and
392 second-site modifiers (Rabinow and Birchler, 1989), and *BEAF-32*, which is also an insulator
393 DNA-binding protein, has been proposed as a possible inverse dosage regulator (Gurudatta et al.,
394 2012; Zhang et al., 2021b), We speculated that the transcription factor *su(Hw)* may also be a
395 dosage-sensitive regulator. The data showed that the transcription levels of *su(Hw)* are
396 up-regulated in all three aneuploidies, and there is a consistent m^6A modification site with
397 significantly down-regulated methylation (Figure 6G). At the same time, the transcripts of this
398 gene have a common alternative 5' splice site (A5SS), and its inclusion levels in trisomies are
399 down-regulated, that is, more short transcript isoforms are generated (Figure 6G). *Ppn* gene
400 encodes an essential extracellular matrix protein that influences cell rearrangements. The
401 expression level of *Ppn* and its m^6A methylation in 5'UTR region are both significantly
402 up-regulated in trisomies (Figure 6—figure supplement 1F). In addition, an alternatively spliced
403 exon is significantly less frequently skipped in all aneuploid *Drosophila* (Figure 6—figure
404 supplement 1G). The third gene, *CG13124*, which may be involved in involved in regulation of
405 translational initiation, is up-regulated in aneuploids. Two m^6A sites in its 5'UTR region are
406 methylated at higher levels in all aneuploid *Drosophila* (Figure 6—figure supplement 1H). Its
407 transcripts also have a common significantly different exon-skipping event (Figure 6—figure
408 supplement 1I).

409 These results indicate that there are complicated relationships among RNA m^6A modification,

410 gene expression, and alternative splicing under the condition of genome imbalance. RNA splicing
411 seems to be more closely related to m^6A methylation than gene transcription. The m^6A sites
412 located in 5'UTR show remarkable changes in methylation levels in aneuploid *Drosophila*, and
413 may be involved in the regulation of some differential alternative splicing events, such as exon
414 skipping.
415

416 **Interactions between m^6A and *Drosophila* Male Specific Lethal (MSL) complex**

417 Previous studies have shown that m^6A components are involved in regulating the alternative
418 splicing of sex-determining gene *Sxl* in *Drosophila*, and the deficiency of m^6A writers or readers
419 will lead to the reduction of female-specific isoforms of *Sxl* (Haussmann et al., 2016; Lence et al.,
420 2016; Kan et al., 2017). *Sxl* is also a direct target of RNA m^6A modification (Kan et al., 2017). We
421 found that *Sxl* transcripts are both differentially methylated and differentially spliced in three
422 kinds of aneuploid *Drosophila* (Figure 7A,B). For trisomy 2L females and metafemales, two
423 common m^6A peaks are significantly up-regulated in the 5'UTR region of *Sxl*. However, trisomy 2L
424 males have a significantly down-regulated m^6A peak in the 5'UTR (Figure 7A). Meanwhile,
425 multiple junctions of *Sxl* transcripts undergo complicated alternative splicing in aneuploid
426 *Drosophila*, including SE, A5SS, alternative 3' splice site (A3SS), and mutually exclusive exons
427 (MXE) types (Figure 7A). By checking the distributions of RNA sequencing reads near the
428 male-specific exon (namely the third exon), it can be observed that there are almost no mapped
429 reads on the third exon in wildtype females, trisomy 2L females, and metafemales, while the
430 reads mapped to the second and fourth exons are highly prevalent (Figure 7B). On the contrary,
431 wildtype males and trisomy 2L males have a substantial number of reads on the third exon,
432 accompanied by a smaller number of reads on the adjacent two exons (Figure 7B). Notably, we
433 found that a small number of RNA-seq reads aligned to the male-specific exon appeared in
434 trisomy 2L females, which was identified as an SE-type differential alternative splicing event (FDR
435 = 7.4e-7; Figure 7B). This variation may be related to the abnormal m^6A methylation levels under
436 the condition of genomic imbalance.

437 The abnormal expression of m^6A components reduces the survival of female *Drosophila*,
438 which is thought to be probably caused by the expression of downstream MSL complex

439 (Haussmann et al., 2016). To investigate the interplay between the MSL complex and m^6A
440 modification, we examined the responses of m^6A regulators in transgenic *Drosophila* strains with
441 MSL2 mutation or overexpression (Figure 7—figure supplement 1A-E; Figure 7C,D). The results
442 revealed significant changes in the expression profiles of m^6A regulators in MSL2 transgenic
443 strains, especially the m^6A reader protein Ythdc1, which increased tens of fold in MSL2
444 knockdown and overexpressed *Drosophila* (Figure 7C,D; Figure 7—figure supplement 1E). We
445 also observed that the trends of Ime4 expression in females and males were the same in
446 MSL2-overexpressed *Drosophila*, whereas there was obvious sexual dimorphism in
447 MSL2-knockdown samples (Figure 7C,D), which may be due to the ectopic assembly of MSL
448 complex in MSL2-overexpressed females (Zhang et al., 2021a). In addition, we also examined the
449 expression levels of MSL2 when *Ythdc1* was knocked down, and found that MSL2 was also
450 significantly increased in females (Figure 7—figure supplement 1F). All these results strongly
451 suggest a potential relationship between MSL2 and Ythdc1. Next, we further compared the
452 overall abundance of m^6A on mRNA in MSL2 transgenic and wildtype *Drosophila* (Figure 7E,F).
453 The results showed that mRNA m^6A levels were significantly decreased with MSL2 knockdown in
454 females and males, but overexpression of MSL2 failed to exert a discernible effect on m^6A
455 abundance (Fig.7E,F).

456 In the next, we investigated the expression of m^6A regulators in aneuploid *Drosophila*
457 overexpressing MSL2, according the results that the MSL complex could be regulated directly or
458 indirectly by m^6A modification, and the sexual dimorphism of RNA m^6A modification in response
459 to aneuploidy. It is found that the transcription levels of m^6A regulators are significantly
460 up-regulated in the brains of most aneuploid larvae that overexpressed MSL2 (Figure 7G; Figure
461 7—figure supplement 1I). These results are not completely consistent with the quantitative
462 results when MSL2 was overexpressed in diploids, which may be related to the effect of
463 unbalanced genomes. We also used TSA-FISH to detect the expression and distribution of m^6A
464 components during embryogenesis in aneuploidies overexpressing MSL2 (Figure 7H; Figure
465 1—figure supplement 2). The subembryonic and subcellular distributions of mRNAs for m^6A
466 methyltransferases and reading protein did not appear to be affected by ectopic expression of
467 MSL2 in aneuploid *Drosophila* embryos (Figure 1—figure supplement 2A-F; Figure 1—figure
468 supplement 2A'-F'). But the relative expression of m^6A components showed diverse dynamics,

469 among which the levels of the most important methyltransferase Ime4 are significantly
470 up-regulated in autosomal trisomy and sex chromosome trisomy with MSL2 overexpression
471 (Figure 7H; Figure 1—figure supplement 2A"-F"). Considering that unbalanced genomes can
472 affect the expression of MSL complex subunits, and the above results show that there is a close
473 relationship between MSL complex and m^6A modification, we speculate that unbalanced
474 genomes may influence the expression of m^6A regulators, possibly through the MSL complex.
475

476 **Relationship of H4K16Ac with m^6A modification**

477 As an important component of the MSL complex, MOF is a histone acetyltransferase that
478 specifically acetylates histone H4 at lysine 16 (H4K16Ac), thereby affecting chromatin structure
479 and functions, and activating transcription (Kind et al., 2008; Conrad et al., 2012). Previous
480 studies have elucidated the regulatory role of m^6A in histone modifications, and histone 3 lysine
481 36 trimethylation (H3K36me3) also plays a role in recruiting methyltransferase complexes to
482 deposit m^6A markers on RNA (Wang et al., 2018; Huang et al., 2019; Li et al., 2020). To investigate
483 the functions of MOF-mediated H4K16Ac on RNA m^6A modification, we analyzed RNA-seq data
484 from *Drosophila* strains overexpressing MOF (Figure 8A; Figure 7—figure supplement 1J-L). We
485 found obvious changes in the expression of m^6A regulators in strains overexpressing MOF, with
486 the levels of almost all m^6A regulators being elevated (Figure 8A). It was also observed that after
487 overexpression of MOF, the increasing trends of m^6A regulators in females and males were not
488 exactly the same, mostly showing more pronounced increases in females, except for Mettl3
489 (Ime4) and dMettl14. According to the results of RT-qPCR, the expression of Ythdc1 was
490 decreased in MOF knockdown strains and increased in MOF overexpression strains (Figure 8B;
491 Figure 7—figure supplement 1J); meanwhile, the expression levels of MOF were significantly
492 reduced in *Ythdc1* neural-knockdown strains (Figure 8C). These results were further verified by
493 polytene chromosome immunofluorescence experiments (Figure 8—figure supplement 1E, F). In
494 males, the expression level of MOF was significantly decreased in *Ythdc1* neural-knockdown
495 *Drosophila*; while in *Ythdc1* neural-knockdown females, the expression level of MOF was not
496 significantly changed compared with wildtype females (Figure 8—figure supplement 1E, F). These
497 results suggest that MOF-mediated acetylation modification can have a certain effect on RNA

498 m^6A methylation in a sexually dimorphic manner, which may be due to the endogenous MSL
499 complex and the imbalance of X chromosome dosage in males.

500 Next, we investigated whether the m^6A reader protein Ythdc1 would also have an effect on
501 the levels of H4K16Ac in *Drosophila*. To this end, we employed western blot analysis to assess the
502 expression patterns of H4K16Ac in *Ythdc1* knockdown *Drosophila* adults (Figure 8D). The
503 subsequent quantitative analysis revealed a significant upregulation of H4K16Ac in both female
504 and male (Figure 8E,F). Furthermore, to substantiate our findings, we conducted polytene
505 chromosome immunofluorescence in third instar larvae (Figure8—figure supplement 1G).
506 Quantitative analysis of these assays in *Ythdc1* knockdown *Drosophila* showed that the changes
507 of H4K16Ac levels also showed sexual dimorphism (Figure 8—figure supplement 1H). In males,
508 knockdown of *Ythdc1* led to a decrease in H4K16Ac level; whereas in females, knockdown of
509 *Ythdc1* did not affect the level of H4K16Ac (Figure 8—figure supplement 1H). These observed
510 changes in H4K16Ac were consistent with the pattern of changes in MOF protein in *Ythdc1*
511 knockdown *Drosophila* strains, suggesting that m^6A modification may affect H4K16Ac levels
512 through the mediation of MOF. Overall, while the alterations in H4K16Ac levels are not uniformly
513 consistent between larvae and adult *Drosophila*, these findings nonetheless demonstrate that
514 the knockdown of *Ythdc1* has a significant impact on the expression levels of H4K16Ac at
515 different stages of development and imply a potential relationship between H4K16Ac with m^6A
516 modification.

517 We analyzed two ChIP-seq datasets (GSE109901 and GSE58768) to study whether m^6A
518 regulator genes (especially *Ythdc1*) are targets of DCC components and H4K16Ac. According to
519 the results, most of the m^6A regulator genes, including *Ythdc1*, contain H4K16Ac peaks in both
520 sexes, all of which are located in the 5' regions (Figure 8G; Figure 8—figure supplement 2); except
521 that *Ime4* shows sexual dimorphism and only contains H4K16Ac peak in females. On the other
522 hand, analysis of ChIP-seq data of MSL2 and MOF in male *Drosophila* showed that most of MSL2
523 and MOF peaks were located on the X chromosome (99.1% of MSL2 peaks and 61.6% of MOF
524 peaks), which may be due to the fact that MSL2 and MOF are mostly tethered to the X
525 chromosome by MSL complex under physiological conditions (Bashaw and Baker 1995; Kelley et
526 al., 1995; Kind et al., 2008; Conrad et al., 2012). Therefore, there is no MSL2 and MOF peak near
527 the m^6A regulator genes which located on the autosomes (Figure 8H; Figure 8—figure

528 supplement 2). These results showed that there is a direct relationship between m^6A regulators
529 and H4K16Ac, but there is no evidence that m^6A regulator genes are direct targets of DCC
530 components. MSL2 and MOF may thereby interact with m^6A regulators in other ways.

531 To further study whether unbalanced genomes are involved in the interaction between m^6A
532 and histone acetylation modification, we also analyzed RNA sequencing data from trisomy 2L
533 *Drosophila* strains overexpressing MOF. The data showed that overexpression of MOF in trisomy
534 2L resulted in significant changes in the expression of m^6A regulators, with a trend different from
535 that observed in diploids (Figure 8A). These results suggest that genomic imbalance might affect
536 the interaction between MOF and m^6A regulators to some extent, and the potential mechanisms
537 require further investigation.

538

539

540 Discussion

541 As an emerging epigenetic modification, RNA m^6A methylation has been found to be involved in
542 almost all aspects of RNA fate and metabolism (Gilbert et al., 2016; Yang et al., 2018). RNA m^6A
543 modification is also closely related to the development of organisms and a variety of human
544 diseases (Barbieri et al., 2017; Zhao et al., 2017; Pinello et al., 2018; Ma et al., 2019; Liu et al.,
545 2021; Shafik et al., 2021). However, the roles of m^6A methylation in development and gene
546 expression of aneuploidy have not been studied yet. Aneuploid variation is usually more
547 detrimental than changes of the entire chromosome set due to genomic imbalance (Birchler and
548 Veitia, 2007, 2012). The global changes of gene regulatory networks in unbalanced genomes
549 involves various epigenetic mechanisms, including histone modification, chromatin remodeling,
550 lncRNAs, microRNAs, etc. (Birchler, 2016; Zhang et al., 2021a, 2023; Shi et al., 2022). This study
551 demonstrated that the expression of m^6A components was altered under genomic imbalance,
552 leading to dynamic changes in the entire methylome. Potential intermediaries by which m^6A
553 modification could affect *trans* regulation and achieve dosage compensation in aneuploid
554 *Drosophila* were also investigated, such as dosage-sensitive modifiers, alternative splicing events,
555 and the MSL complex.

556 Our experiments show that the expression levels of most m^6A component genes are

557 significantly down-regulated in aneuploid *Drosophila* larvae (Figure 1A; Figure 1—figure
558 supplement 1C). Depletion of m^6A components interferes with the development of animals and
559 plants, especially leading to impaired self-renewal and differentiation of embryonic stem cells,
560 defects in embryonic development, and even early embryonic lethality (Granadino et al., 1990;
561 Horiuchi et al., 2006; Raffel et al., 2007; Luo et al., 2014; Wang Y et al., 2014; Geula et al., 2015).
562 We demonstrated by TSA-FISH that appropriate temporal and spatial specific distributions of the
563 transcripts for m^6A components are vital during *Drosophila* embryogenesis (Figure 1C-F; Figure
564 1—figure supplement 2). The abnormal expression of m^6A-related genes may affect the
565 development of aneuploid embryos.

566 In previous studies, the abundance of m^6A modification is usually positively correlated with
567 the number of m^6A peaks and m^6A-marked genes (Luo et al., 2014; Zhu et al., 2023). However,
568 our results obviously did not conform to this rule, with higher m^6A abundance and fewer
569 MeRIP-Seq peaks in aneuploids (Figure 2A-C). This reflects the complexity and heterogeneity of
570 m^6A modification. We suspect that in aneuploidy many RNAs may be lost that are methylated at
571 a low level in wildtype, and possess a higher proportion of highly methylated RNAs. Analysis of
572 the expression levels at each m^6A site confirmed our hypothesis (Figure 2D). Thus, this
573 phenomenon represents an imbalance in m^6A methylation caused by aneuploidy. In addition, it is
574 worth noting that due to the limitation of the larval samples, our detection of the overall
575 abundance of m^6A in aneuploidy is carried out for total RNA, including all types of RNA such as
576 mRNA, lncRNA, and rRNA, and may be slightly different from detection of mRNA only. However,
577 according to the results of m^6A abundance detection in *Drosophila* adult heads, the enrichment
578 or non-enrichment of mRNA from total RNA did not make a substantive difference in the results.

579

580 The distribution of m^6A sites on gene features, m^6A consensus motifs, biotypes of
581 m^6A-marked genes, enriched functions and pathways of methylated genes in aneuploidies are
582 similar to those in wildtype. We also found that genes highly methylated in all genotypes are
583 enriched for transcription factors (Figure 2I). It is consistent with previous studies suggesting that
584 transcription regulatory genes may be preferentially targeted by m^6A (Kan et al., 2017).

585 We also analyzed the characteristics of DMPs and DMP-associated genes in trisomies. By
586 observing the distributions of MeRIP-Seq reads around DMP sites, it can be found that the

587 densities of m^6A-marked reads on chromosome 2L are relatively higher in trisomy 2L females and
588 males (Figure 3F,G). Meanwhile, metafemales with triple X have a higher density of m^6A-marked
589 reads on chromosome X (Figure 3H). Previous studies have found that there is dosage
590 compensation for *cis*-genes in autosomal and sex chromosome aneuploid *Drosophila*, and the
591 expression of most genes on varied chromosomes approaches diploid levels (Sun et al., 2013b,c).
592 Therefore, the up-regulation of m^6A levels is not directly caused by the increased number of
593 chromosomes. A recent study found that the selective enrichment of m^6A methylation may play a
594 role as a transcript degradation signal in dosage compensation in mammals (Rücklé et al., 2023).
595 Therefore, we speculate that changes in m^6A levels in aneuploid *Drosophila* may affect its dosage
596 compensation and inverse dosage effect by regulating the stability of the transcripts. In addition,
597 more up-regulated DMPs are detected in trisomy 2L males and metafemales, while trisomy 2L
598 females have more down-regulated DMPs (Figure 3A-D). Combined with the fact that the survival
599 rate of trisomy 2L female larvae is relatively lower than that of the other two trisomies, it can be
600 speculated that the regulation of DMPs may affect the survival and development of aneuploid
601 *Drosophila*.

602 Gene expression in unbalanced genomes is extensively modulated (Sun et al., 2013b,c; Hou et
603 al., 2018; Raznahan et al., 2018; Shi et al., 2021; Yang et al., 2021; Zhang et al., 2021b; San Roman
604 et al., 2023). Previous studies have analyzed the transcriptome data of autosomal and sex
605 chromosome trisomic *Drosophila*, and found that most of the genes on the triple chromosomes
606 were compensated, and the ratios of their expression levels to wildtype were approximately 1;
607 meanwhile, the expression of genes on other chromosomes was close to two-thirds of that of the
608 wildtype, which was called an inverse dosage effect (Sun et al., 2013b,c; Zhang et al., 2021b). We
609 investigated the relationships between genes with different m^6A methylation status and genes
610 modulated by classical dosage-related effects (Figure 5F-H). The results showed that for
611 aneuploid females, genes methylated in both trisomy and control are significantly enriched in
612 dosage compensated *cis* genes and inverse dosage effect *trans* genes, and genes not methylated
613 at all are enriched in dosage effect genes. However, in aneuploid males, methylated genes are
614 associated with gene dosage effect (Figure 5F-H). We also found that the proportion of 5'UTR
615 m^6A peaks on dosage compensation and inverse dosage effect genes are increased in aneuploid
616 females (Figure 5I-K). These results provide evidence of sexual dimorphism in the relationships

617 between RNA m^6A modification and dosage-related effects. m^6A located in the 5'UTR generally
618 shows higher tissue specificity and richer dynamic changes, and may have unique regulatory
619 functions (Dominissini et al., 2012; Meyer and Jaffrey, 2014; Gilbert et al., 2016). The increased
620 proportion of m^6A in the 5'UTR of genes with classical dosage-related effects in aneuploidies
621 suggests that m^6A modification may be involved in the regulation of dosage-dependent genes.

622 Dosage-related effects of aneuploidy are thought to be caused by dosage-sensitive genes (Shi
623 et al., 2021; Yang et al., 2021). Some dosage-sensitive regulators have been identified in
624 *Drosophila*, and changes in the dosage of individual regulatory genes can mimic the effects of
625 aneuploidy in the whole genome (Birchler et al., 2001; Xie and Birchler, 2012; Zhang et al., 2021b).
626 Most dosage-sensitive regulators are transcription factors, signal transduction components, and
627 chromatin proteins, which have in common being members of macromolecular complexes or
628 having multicomponent interactions (Birchler et al., 2001; Birchler and Veitia, 2007). We studied
629 the m^6A modification of dosage-dependent genes and their protein-protein interaction networks
630 in aneuploid *Drosophila* (Figure 5—figure supplement 1). The results showed that there are
631 complex interactions between dosage-sensitive regulators and differentially expressed genes.
632 Among them, most of the DEGs located on the unvaried chromosomes are down-regulated,
633 indicating that the dosage-sensitive regulators mainly have negative effects on *trans* target genes.
634 There are more regulatory genes with up-regulated DMPs than down-regulated DMPs in all three
635 aneuploidies, and many of the regulators with up-regulated methylation are connected with
636 interactors that have down-regulated expression.

637 We comprehensively analyzed the relationships among RNA m^6A modification, gene
638 expression levels, and alternative splicing. The data showed that differential m^6A methylation
639 under genomic imbalance appeared to be more closely associated with differential alternative
640 splicing (Figure 5A-C; Figure 6A-C). This phenomenon is reasonable because the mutation or
641 knockout of *Ime4*, *dMettl14*, *fl(2)d*, and *Ythdc1* has been found to affect a large number of
642 alternative splicing events in *Drosophila*, and *fl(2)d* itself is thought to encode a splicing factor
643 (Penn et al., 2008; Haussmann et al., 2016; Lence et al., 2016). A small set of transcripts are
644 simultaneously differentially m^6A methylated, differentially expressed, and differentially
645 alternative spliced in aneuploidies, including the transcription factor *su(Hw)*, which may be a
646 dosage-sensitive regulator (Figure 6G-H). Besides, m^6A modification in the 5'UTR regions may

647 play a special role in some differential alternative splicing events (Figure 6—figure supplement
648 1F-I).

649 RNA m^6A modification in *Drosophila* has been shown to be involved in the alternative splicing
650 of *Sxl* (Lence et al., 2017). The deletion of some m^6A components in females will result in a
651 reduction of female-specific splicing of *Sxl* and an increase of the inclusion of the third exon,
652 along with phenotypic sexual transformation (Haussmann et al., 2016; Lence et al., 2016; Kan et
653 al., 2017). We found that *Sxl* transcripts of aneuploid *Drosophila* are both differentially m^6A
654 methylated and differentially spliced (Figure 7A-B). Among multiple alternative splicing events,
655 trisomy 2L females have a higher level of the third exon inclusion compared with wildtype
656 females (Figure 7B), which may be related to the differential methylation at 5'UTR of the *Sxl*
657 transcripts.

658 Some studies proposed that the deletion of RNA m^6A methyltransferase Ime4 harms the
659 survival of female *Drosophila* because of the insufficient inhibition of *msl-2* caused by decreased
660 *Sxl* levels, which in turn leads to up-regulation of X-linked genes (Haussmann et al., 2016).
661 However, other studies have found that the expression of genes on the X chromosome in females
662 with ectopic expression of MSL2 does not increase twofold, that is, the MSL complex does not
663 directly mediate dosage compensation, and the global inverse dosage effect caused by the
664 imbalance of sex chromosomes is the basis for dosage compensation (Birchler, 1981, 2016; Sun et
665 al., 2013a). Therefore, the lethality of the lack of m^6A in female *Drosophila* may not be directly
666 caused by up-regulation of X-linked genes through ectopic assembly of MSL complex, and the
667 specific reasons need to be further studied.

668 The functions of MSL complex in dynamic regulation of global gene expression in aneuploid
669 genomes has been described (Zhang et al., 2021a). Here, we found that MSL2, a structure
670 component of MSL complex, not only affects the expression of m^6A regulators, but also
671 influences the overall abundance of mRNA m^6A in *Drosophila* (Figure 7C-F), proving a close
672 relationship between the MSL complex and RNA m^6A modification. In addition, under the
673 condition of genomic imbalance, the relative expression of m^6A components was also changed in
674 larvae and embryos of MSL2-overexpressed trisomies (Figure 7G,H). Another component of the
675 MSL complex, MOF, which mediates histone acetylation and transcriptional activation (Kind et al.,
676 2008; Conrad et al., 2012), is also closely associated with the m^6A reader Ythdc1. Overexpression

677 of MOF increased the expression of Ythdc1 (Figure 8A,B), and in turn, knockdown of *Ythdc1*
678 influenced the expression of MOF and the level of H4K16Ac catalyzed by it (Figure 8C-F; Figure
679 8—figure supplement 1G,H). It is worth noting that the rationale behind the variable expression
680 levels of H4K16Ac in *Ythdc1* knockdown *Drosophila* across different developmental stages merits
681 further investigation. These results demonstrate complicated interactions between RNA m^6A
682 methylation and the MSL complex in unbalanced genomes, which may affect the gene expression,
683 sexual dimorphism, development and survival of aneuploid *Drosophila*.
684
685

686 # Materials and methods

687 ## Key resources table

688 Softwares used in this study:

Resource	Designation	Source or reference
software, algorithm	R v4.2.2	http://www.R-project.org
software, algorithm	trim-galore v0.6.10	https://www.bioinformatics.babraham.ac.uk/projects/trim_galore/
software, algorithm	FastQC v0.12.1	https://www.bioinformatics.babraham.ac.uk/projects/fastqc/
software, algorithm	HISAT2 v2.2.1	Kim et al., 2019
software, algorithm	StringTie v2.1.5	Pertea et al., 2015
software, algorithm	exomePeak2 v1.10.0	Meng et al., 2013
software, algorithm	HOMER v4.11	Heinz et al., 2010
software, algorithm	DiffBind v3.8.4	Stark and Brown, 2013
software, algorithm	ChIPseeker v1.34.1	Yu et al., 2015
software, algorithm	deepTools v3.5.4	Ramírez et al., 2014
	rMATS v4.2.0	Shen et al., 2014
software, algorithm	ggplot2 v3.4.0	Villanueva and Chen, 2019
software, algorithm	clusterProfiler v4.6.0	Wu et al., 2021
software, algorithm	org.Dm.eg.db v3.16.0	https://www.bioconductor.org/
software, algorithm	DESeq2 v1.38.2	Love et al., 2014
software, algorithm	Integrative Genomics Viewer v2.12.0	Thorvaldsdóttir et al., 2013
software, algorithm	Fiji v1.53c	Schindelin et al., 2012
software, algorithm	AnimalTFDB	Hu et al., 2019

689

690 Antibodies used in this study:

Antibody	Manufacturer	Product #	RRID #
Mouse anti-SXL	Developmental Studies Hybridoma Bank	M18-s	AB_528464
Goat anti-MSL2	Santa Cruz	sc-32459	AB_672213
Goat anti-MOF	Santa Cruz	sc-22351	AB_670132
Rabbit anti-H3	Novus	NB500-171	AB_10001790
Rabbit anti-H4K16Ac	EMD Millipore	07-329	AB_310525
Alexa Fluor 488/594	Jackson Immuno Research	N/A	N/A
HRP-conjugated Mouse anti-rabbit IgG	Sangon Biotech	D110065	N/A
Biotin-Conjugated Mouse Monoclonal Anti-Digoxigenin antibody	Jackson Immuno Research	200-062-156	AB_2339017
Streptavidin-HRP	Invitrogen	S991	N/A
Cyanine 3 Tyramide	Akoya Biosciences	FP1046	N/A

691

692 ## *Drosophila* stocks and genetic crosses

693 The *Drosophila* strains mentioned in this study were all maintained and crossed in our laboratory.
694 The crossing methods have been described previously (Zhang et al., 2021a). Trisomy
695 chromosome 2 left arm (2L) female and male third instar larvae were obtained from the cross of
696 *y; C(2L)dp; F(2R) bw* females and Canton S males. The metafemale larvae were obtained from the
697 cross of *C(1)DX, ywf/winscy* females and Canton S males. Aneuploidies overexpressing MSL2 were
698 generated from the crosses of *Drosophila* with compound chromosomes and MSL2 homozygotes.
699 The MSL2 transgene strain was constructed and validated in a previous study (Sun et al., 2013a).
700 All *Drosophila* strains were cultured on cornmeal dextrose medium at 25°C. Genes and
701 chromosomal balancers are described in Flybase (https://flybase.org/).

702

703 ## RNA m^6A methylation quantification

704 Total RNA was extracted from *Drosophila* larvae using TRIzol Reagent (Invitrogen) and mRNA was
705 isolated using the Dynabeads mRNA purification kit (Invitrogen, 61006) to detect the abundance
706 of m^6A. The relative quantification of m^6A methylation was performed using EpiQuik m^6A RNA
707 Methylation Quantification Kit (Colorimetric) (Epigentek, NY, USA, Cat # P-9005). Specifically, 80

708 µl of Binding Solution was first added to each well of the plate, and 200 ng of total RNA or mRNA
709 samples, 2 µl of Negative Control, or 2 µl of diluted Positive Control were added to the designed
710 wells. Subsequently, the plate was incubated at 37°C for 90 min. After washing with Wash Buffer,
711 50 µl of Capture Antibody, 50 µl of Detection Antibody, and 50 µl of Enhancer Solution were
712 added to each well in order, and wells were emptied before adding a new solution each time.
713 Finally, 100 µl of Developer Solution and Stop Solution were added to each well away from light,
714 and the absorbance was read on a microplate reader at a wavelength of 450 nm.
715

716 m^6A methylated RNA immunoprecipitation sequencing (MeRIP-Seq)

717 The MeRIP-Seq service was provided by Cloudseq Biotech Inc. (Shanghai, China), and this
718 technology was developed on the basis of published experimental methods (Meyer et al., 2012).
719 In brief, *Drosophila* larvae of five genotypes, each with two biological replicates, were collected
720 for sequencing. Ribosomal RNAs were removed from total RNA using Ribo-Zero rRNA Removal
721 Kits (Illumina, USA). Immunoprecipitation of m^6A RNA was performed using GenSeq® m^6A RNA IP
722 kit (GenSeq, Shanghai, China). The NEBNext® Ultra II Directional RNA Library Prep kit (New
723 England Biolabs, USA) was used for RNA sequencing library construction. High-throughput
724 sequencing was performed using Illumina NovaSeq 6000 sequencers with the paired-end 150 bp
725 protocol.
726

727 Analysis of MeRIP-Seq data

728 The raw sequencing data was first filtered by Trim Galore (version 0.6.10)
729 (https://www.bioinformatics.babraham.ac.uk/projects/trim_galore/) to remove adapters and
730 low-quality reads. The quality of the data was then assessed by FastQC (version 0.12.1)
731 (https://www.bioinformatics.babraham.ac.uk/projects/fastqc/). Subsequently, clean reads were
732 aligned to the *Drosophila* reference genome (Drosophila_melanogaster.BDGP6.32.dna.toplevel.fa,
733 downloaded from the Ensembl database) using HISAT2 (version 2.2.1) (Kim et al., 2019). Next,
734 The R package exomePeak2 (version 1.10.0) (Meng et al., 2013) was used for m^6A peak calling
735 (the screening criteria were log2FC ≥ 1, RPM.IP ≥ 0.5, and score ≥ 5). Motif analysis was
736 performed using HOMER (version 4.11) (Heinz et al., 2010). Differentially methylated peaks were

737 analyzed by the R package DiffBind (version 3.8.4) (Stark and Brown, 2013), which employs the
738 DESeq2 (Love et al., 2014) method. m^6A peaks with a p-value of 0.1 or less were considered as
739 differentially methylated peaks (DMPs). ChIPseeker (version 1.34.1) (Yu et al., 2015) was used to
740 annotate the peaks, and plotted some of the figures. The profiles and heatmaps of MeRIP-Seq
741 reads around DMPs were generated by deepTools (version 3.5.4) (Ramírez et al., 2014). The signal
742 distribution on the genome was visualized using the Integrative Genomics Viewer (IGV) software
743 (version 2.12.0) (Thorvaldsdóttir et al., 2013).
744

745 **RNA sequencing data and analysis**

746 The RNA-seq data of aneuploid *Drosophila* used in this article were generated in a previous study
747 (Zhang et al., 2023) and can be downloaded from the Gene Expression Omnibus (GEO) database
748 (GSE233534). Genome mapping of sequencing data and gene expression quantification were
749 carried out through HISAT2-StringTie pipeline (Pertea et al., 2015; Kim et al., 2019). Differential
750 alternative splicing events were identified by rMATS (version 4.2.0) program (Shen et al., 2014)
751 (with the parameters of -t paired --readLength 150 --cstat 0.0001 --libType fr-firststrand). The
752 method of generating the ratio distributions of gene expression changes was as described
753 previously (Zhang et al., 2022). The plots were generated using ggplot2 (version 3.4.0) (Villanueva
754 and Chen, 2019) in the R program (version 4.2.2). Differential expression analysis was performed
755 by DESeq2 (version 1.38.2) (Love et al., 2014), and the threshold was set to adjusted p-value ≤
756 0.05. The functional enrichment analysis was performed by ClusterProfiler (version 4.6.0) (Wu et
757 al., 2021) based on org.Dm.eg.db (version 3.16.0) from Bioconductor
758 (https://www.bioconductor.org/). The Kyoto Encyclopedia of Genes and Genomes (KEGG)
759 pathway data was obtained from the network (https://www.kegg.jp/). The list of transcription
760 factors of *Drosophila* was downloaded from AnimalTFDB (Hu et al., 2019). Protein-protein
761 interaction (PPI) relationships were obtained from the STRING database (Szklarczyk et al., 2019).
762

763 **Real-time quantitative PCR**

764 Total RNA of *Drosophila* whole larvae, larval brains, or adult heads was extracted using TRIzol
765 Reagent (Invitrogen), and reverse transcription was done with *TransScript* one-step gDNA

766 Removal and cDNA Synthesis SuperMix (TransGen Biotech). The sequences of primers designed
767 for RT-qPCR were listed in Figure 1—figure supplement 1A. The usability of these primers was
768 verified by agarose gel electrophoresis (Figure 1—figure supplement 1B). The real-time PCR was
769 performed with *TransStart* Tip Green qPCR SuperMix (+ Dye II) (TransGen Biotech) using ABI
770 QuantStudio 6 Flex Real-Time PCR System. Relative quantification of gene expression was
771 determined using the $2^{-\Delta\Delta Ct}$ method.
772

773 **Fluorescence *in situ* hybridization (FISH) of *Drosophila* embryos**

774 Collection of *Drosophila* embryos and fluorescence *in situ* hybridization were performed as
775 previously described (Jandura et al., 2017; Zhang et al., 2021a). The probe primers containing
776 flanking T7 promoter elements were listed in Figure 1—figure supplement 1D. After PCR
777 amplification and *in vitro* transcription, their products were examined by agarose gel
778 electrophoresis (Figure 1—figure supplement 1E). Digoxygenin (DIG)-labelled antisense RNA
779 probes were hybridized to transcripts of interest, and then detected using a succession of
780 anti-DIG antibody conjugated to biotin, streptavidin conjugated to horseradish peroxidase (HRP)
781 and fluorescently conjugated tyramide. This hierarchical process can greatly enhance the probe
782 signals and is referred to as a tyramide signal amplification (TSA) system. All images were
783 acquired with a Zeiss LSM880 laser confocal fluorescence microscope using ZEN software. The
784 same probes for relative fluorescence intensity analysis were photographed using the same
785 parameters. Fluorescence images were processed and analyzed using Fiji (version 1.53c)
786 (Schindelin et al., 2012).
787

788 **Polytene chromosomes immunostaining**

789 Salivary gland chromosomes immunostaining was performed as previously described (Zhang et
790 al., 2021a). Briefly speaking, the salivary glands from third-instar larvae were first fixed in 3.7%
791 formaldehyde for 1 min, and then dissociated with 50% acetic acid for 5 min. Polytene
792 chromosomes were treated with the following primary antibodies at a dilution of 1:100: anti-SXL
793 (Developmental Studies Hybridoma Bank, M18-s), anti-MSL2 (Santa Cruz, sc-32459), anti-MOF
794 (Santa Cruz, sc-22351), and anti-H4K16Ac (EMD Millipore, 07-329). Finally,

795 fluorescence-conjugated secondary antibodies (Alexa Fluor 488 and Alexa Fluor 594, Jackson
796 Immuno Research) were used for detection.
797

798 **Histone extraction and Western Blotting**

799 *Drosophila* adults were ground and lysed in Triton Extraction Buffer (PBS at pH 7.4 with 0.5%
800 Triton X-100, 0.5 mM phenymethylsulfonyl fluoride, and 0.02% sodium butyrate) and histones
801 were acid-extracted in 0.2 N HCl overnight. Acid-extracted histones were then run on a 12%
802 Tris-Glycine gel and blotted onto a PVDF membrane. Antibodies for Histone H3 (NB500-171,
803 Novus) and H4K16Ac (07-329, Sigma) were all incubated at a dilution of 1:1000 in 5% skim milk
804 powder solution. Westerns blots were imaged and protein levels quantified using the ImageJ
805 software.
806

807 ## Acknowledgements

808 This work was supported by National Natural Science Foundation of China (Grant No. 32070566)
809 to L.S. We thank James A.Birchler for revising the manuscript.
810
811

812 ## Additional information

813 ## Funding

Funder	Grant reference number	Author
National Natural Science Foundation of China	No. 32070566	Lin Sun

814

815 ## Author contributions

816 Shuai Zhang: Methodology, Investigation, Data Curation, Formal analysis, Writing - Original Draft,
817 Writing - Review & Editing, Visualization. Ruixue Wang, Methodology, Investigation, Validation,
818 Writing - Original Draft, Writing - Review & Editing, Visualization. Kun Luo, Methodology,
819 Investigation, Validation, Writing - Review & Editing, Visualization. Shipeng Gu, Methodology,

Investigation, Writing - Review & Editing, Visualization. Xinyu Liu, Methodology, Investigation, Validation, Writing - Original Draft. Junhan Wang: Methodology, Investigation, Formal analysis. Ludan Zhang: Methodology, Investigation, Validation. Lin Sun: Conceptualization, Writing - Original Draft, Writing - Review & Editing, Supervision, Project administration, Funding acquisition. All authors have read and approved the final manuscript.

Additional files

Supplementary files

Supplementary File 1

Data availability

All raw and processed sequencing data generated in this study have been submitted to the NCBI Gene Expression Omnibus (GEO; https://www.ncbi.nlm.nih.gov/geo/) under accession number GSE253401. The previously published RNA-seq data used in this study are available at the GEO repository under the accession number GSE233534. The previously published ChIP-seq data used in this study are available at the GEO repository under the accession number GSE109901 and GSE58768.

The following datasets were generated:

Author(s)	Year	Dataset title	Dataset URL	Database and Identifier
Zhang S, Liu X, Wang R, Wang J, Zhang L, Sun L	2024	Dynamics and regulatory roles of RNA m^6A methylation in unbalanced genomes	https://www.ncbi.nlm.nih.gov/geo/query/acc.cgi?acc=GSE253401	NCBI Gene Expression Omnibus, GSE253401

The following previously published datasets were used:

Author(s)	Year	Dataset title	Dataset URL	Database and Identifier
Zhang S, Wang R, Zhu X, Zhang L, Liu X, Sun L	2024	Characteristics and expression of lncRNA in *Drosophila* aneuploidy	https://www.ncbi.nlm.nih.gov/geo/query/acc.cgi?acc=GSE233534	NCBI Gene Expression Omnibus, GSE233534

Renschler G, Richard G, Valsecchi CIK, Toscano S et al.	2018	Facultative dosage compensation of developmental genes on autosomes in *Drosophila* and mammals	https://www.ncbi.nlm.nih.gov/geo/query/acc.cgi?acc=GSE109901	NCBI Gene Expression Omnibus, GSE109901
Figueiredo ML, Kim M, Philip P, Allgardsson A, Stenberg P, Larsson J	2014	Non-coding *roX* RNAs prevent the binding of the MSL-complex to heterochromatic regions	https://www.ncbi.nlm.nih.gov/geo/query/acc.cgi?acc=GSE58768	NCBI Gene Expression Omnibus, GSE58768

References

Barbieri, I., Tzelepis, K., Pandolfini, L., Shi, J., Millan-Zambrano, G., Robson, S. C., Aspris, D., Migliori, V., Bannister, A. J., Han, N., De Braekeleer, E., Ponstingl, H., Hendrick, A., Vakoc, C. R., Vassiliou, G. S., & Kouzarides, T. (2017). Promoter-bound METTL3 maintains myeloid leukaemia by m(6)A-dependent translation control. *Nature*, *552*(7683), 126-131. https://doi.org/10.1038/nature24678

Bashaw, G. J., & Baker, B. S. (1995). The *msl-2* dosage compensation gene of *Drosophila* encodes a putative DNA-binding protein whose expression is sex specifically regulated by *Sex-lethal*. Development, 121(10), 3245-3258. doi:10.1242/dev.121.10.3245

Ben-David, U., & Amon, A. (2020). Context is everything: aneuploidy in cancer. *Nature Reviews Genetics*, *21*(1), 44-62. https://doi.org/10.1038/s41576-019-0171-x

Birchler, J. A. (1981). The genetic basis of dosage compensation of alcohol dehydrogenase-1 in maize. *Genetics*, *97*(3-4), 625-637. https://www.ncbi.nlm.nih.gov/pubmed/17249082

Birchler, J. A. (2016). Parallel Universes for Models of X Chromosome Dosage Compensation in *Drosophila*: A Review. *Cytogenetic and Genome Research*, *148*(1), 52-67. https://doi.org/10.1159/000445924

Birchler, J. A., Bhadra, U., Bhadra, M. P., & Auger, D. L. (2001). Dosage-dependent gene regulation in multicellular eukaryotes: implications for dosage compensation, aneuploid syndromes, and quantitative traits. *Developmental Biology*, *234*(2), 275-288.

863 https://doi.org/10.1006/dbio.2001.0262
864 Birchler, J. A., & Veitia, R. A. (2007). The gene balance hypothesis: from classical genetics to
865 modern genomics. *Plant Cell*, *19*(2), 395-402. https://doi.org/10.1105/tpc.106.049338
866 Birchler, J. A., & Veitia, R. A. (2012). Gene balance hypothesis: connecting issues of dosage
867 sensitivity across biological disciplines. *Proceedings of the National Academy of Sciences of*
868 *the United States of America*, *109*(37), 14746-14753.
869 https://doi.org/10.1073/pnas.1207726109
870 Birchler, J. A., & Veitia, R. A. (2021). One Hundred Years of Gene Balance: How Stoichiometric
871 Issues Affect Gene Expression, Genome Evolution, and Quantitative Traits. *Cytogenetic and*
872 *Genome Research*, *161*(10-11), 529-550. https://doi.org/10.1159/000519592
873 Chiarle, R. (2021). Solving the chromosome puzzle of aneuploidy in cancer. *Genes Dev*, *35*(15-16),
874 1073-1075. https://doi.org/10.1101/gad.348773.121
875 Conrad, T., Cavalli, F. M. G., Holz, H., Hallacli, E., Kind, J., Ilik, I., Vaquerizas, J. M., Luscombe, N. M.,
876 & Akhtar, A. (2012). The MOF Chromobarrel Domain Controls Genome-wide H4K16
877 Acetylation and Spreading of the MSL Complex. *Developmental Cell*, *22*(3), 610-624.
878 https://doi.org/10.1016/j.devcel.2011.12.016
879 Disteche, C. M. (2016). Dosage compensation of the sex chromosomes and autosomes. *Semin*
880 *Cell Dev Biol*, *56*, 9-18. https://doi.org/10.1016/j.semcdb.2016.04.013
881 Dominissini, D., Moshitch-Moshkovitz, S., Schwartz, S., Salmon-Divon, M., Ungar, L., Osenberg, S.,
882 Cesarkas, K., Jacob-Hirsch, J., Amariglio, N., Kupiec, M., Sorek, R., & Rechavi, G. (2012).
883 Topology of the human and mouse m6A RNA methylomes revealed by m6A-seq. *Nature*,
884 *485*(7397), 201-206. https://doi.org/10.1038/nature11112
885 Geula, S., Moshitch-Moshkovitz, S., Dominissini, D., Mansour, A. A., Kol, N., Salmon-Divon, M.,
886 Hershkovitz, V., Peer, E., Mor, N., Manor, Y. S., Ben-Haim, M. S., Eyal, E., Yunger, S., Pinto, Y.,
887 Jaitin, D. A., Viukov, S., Rais, Y., Krupalnik, V., Chomsky, E., . . . Hanna, J. H. (2015). Stem cells.
888 m6A mRNA methylation facilitates resolution of naive pluripotency toward differentiation.
889 *Science*, *347*(6225), 1002-1006. https://doi.org/10.1126/science.1261417
890 Gilbert, W. V., Bell, T. A., & Schaening, C. (2016). Messenger RNA modifications: Form, distribution,
891 and function. *Science*, *352*(6292), 1408-1412. https://doi.org/10.1126/science.aad8711
892 Granadino, B., Campuzano, S., & Sanchez, L. (1990). The *Drosophila melanogaster fl(2)d* gene is

needed for the female-specific splicing of *Sex-lethal* RNA. *EMBO Journal*, *9*(8), 2597-2602. https://doi.org/DOI 10.1002/j.1460-2075.1990.tb07441.x

Gurudatta, B. V., Ramos, E., & Corces, V. G. (2012). The BEAF insulator regulates genes involved in cell polarity and neoplastic growth. *Developmental Biology*, *369*(1), 124-132. https://doi.org/10.1016/j.ydbio.2012.06.013

Haussmann, I. U., Bodi, Z., Sanchez-Moran, E., Mongan, N. P., Archer, N., Fray, R. G., & Soller, M. (2016). m(6)A potentiates *Sxl* alternative pre-mRNA splicing for robust *Drosophila* sex determination. *Nature*, *540*(7632), 301-304. https://doi.org/10.1038/nature20577

Heinz, S., Benner, C., Spann, N., Bertolino, E., Lin, Y. C., Laslo, P., Cheng, J. X., Murre, C., Singh, H., & Glass, C. K. (2010). Simple Combinations of Lineage-Determining Transcription Factors Prime *cis*-Regulatory Elements Required for Macrophage and B Cell Identities. *Molecular Cell*, *38*(4), 576-589. https://doi.org/10.1016/j.molcel.2010.05.004

Hongay, C. F., & Orr-Weaver, T. L. (2011). *Drosophila* Inducer of MEiosis 4 (*IME4*) is required for Notch signaling during oogenesis. *Proceedings of the National Academy of Sciences of the United States of America*, *108*(36), 14855-14860. https://doi.org/10.1073/pnas.1111577108

Horiuchi, K., Umetani, M., Minami, T., Okayama, H., Takada, S., Yamamoto, M., Aburatani, H., Reid, P. C., Housman, D. E., Hamakubo, T., & Kodama, T. (2006). Wilms' tumor 1-associating protein regulates G2/M transition through stabilization of cyclin A2 mRNA. *Proceedings of the National Academy of Sciences of the United States of America*, *103*(46), 17278-17283. https://doi.org/10.1073/pnas.0608357103

Hou, J., Shi, X., Chen, C., Islam, M. S., Johnson, A. F., Kanno, T., Huettel, B., Yen, M. R., Hsu, F. M., Ji, T., Chen, P. Y., Matzke, M., Matzke, A. J. M., Cheng, J., & Birchler, J. A. (2018). Global impacts of chromosomal imbalance on gene expression in *Arabidopsis* and other taxa. *Proceedings of the National Academy of Sciences of the United States of America*, *115*(48), E11321-E11330. https://doi.org/10.1073/pnas.1807796115

Hu, H., Miao, Y. R., Jia, L. H., Yu, Q. Y., Zhang, Q., & Guo, A. Y. (2019). AnimalTFDB 3.0: a comprehensive resource for annotation and prediction of animal transcription factors. *Nucleic Acids Research*, *47*(D1), D33-D38. https://doi.org/10.1093/nar/gky822

Huang, A. C., Olson, S. B., & Maslen, C. L. (2021). A Review of Recent Developments in Turner Syndrome Research. *J Cardiovasc Dev Dis*, *8*(11), 475-491.

https://doi.org/10.3390/jcdd8110138

Huang, H., Weng, H., Zhou, K., Wu, T., Zhao, B. S., Sun, M., Chen, Z., Deng, X., Xiao, G., Auer, F., Klemm, L., Wu, H., Zuo, Z., Qin, X., Dong, Y., Zhou, Y., Qin, H., Tao, S., Du, J., . . . Chen, J. (2019). Histone H3 trimethylation at lysine 36 guides m(6)A RNA modification co-transcriptionally. *Nature*, *567*(7748), 414-419. https://doi.org/10.1038/s41586-019-1016-7

Jaenisch, R., & Bird, A. (2003). Epigenetic regulation of gene expression: how the genome integrates intrinsic and environmental signals. *Nature Genetics*, *33 Suppl*, 245-254. https://doi.org/10.1038/ng1089

Jandura, A., Hu, J., Wilk, R., & Krause, H. M. (2017). High Resolution Fluorescent *In Situ* Hybridization in Drosophila Embryos and Tissues Using Tyramide Signal Amplification. *J Vis Exp*, *128*(128), 56281. https://doi.org/10.3791/56281

Jordan, W., Rieder, L. E., & Larschan, E. (2019). Diverse Genome Topologies Characterize Dosage Compensation across Species. *Trends in Genetics*, *35*(4), 308-315. https://doi.org/10.1016/j.tig.2019.02.001

Kan, L., Grozhik, A. V., Vedanayagam, J., Patil, D. P., Pang, N., Lim, K. S., Huang, Y. C., Joseph, B., Lin, C. J., Despic, V., Guo, J., Yan, D., Kondo, S., Deng, W. M., Dedon, P. C., Jaffrey, S. R., & Lai, E. C. (2017). The m(6)A pathway facilitates sex determination in *Drosophila*. *Nat Commun*, *8*, 15737. https://doi.org/10.1038/ncomms15737

Kelley, R. L., Solovyeva, I., Lyman, L. M., Richman, R., Solovyev, V., & Kuroda, M. I. (1995). Expression of *msl-2* causes assembly of dosage compensation regulators on the X chromosomes and female lethality in *Drosophila*. Cell, 81(6), 867-877. doi:10.1016/0092-8674(95)90007-1

Kim, D., Paggi, J. M., Park, C., Bennett, C., & Salzberg, S. L. (2019). Graph-based genome alignment and genotyping with HISAT2 and HISAT-genotype. *Nature Biotechnology*, *37*(8), 907-915. https://doi.org/10.1038/s41587-019-0201-4

Kind, J., Vaquerizas, J. M., Gebhardt, P., Gentzel, M., Luscombe, N. M., Bertone, P., & Akhtar, A. (2008). Genome-wide analysis reveals MOF as a key regulator of dosage compensation and gene expression in *Drosophila*. *Cell*, *133*(5), 813-828. https://doi.org/10.1016/j.cell.2008.04.036

Lecuyer, E., Yoshida, H., Parthasarathy, N., Alm, C., Babak, T., Cerovina, T., Hughes, T. R., Tomancak,

953 P., & Krause, H. M. (2007). Global analysis of mRNA localization reveals a prominent role in
954 organizing cellular architecture and function. *Cell*, *131*(1), 174-187.
955 https://doi.org/10.1016/j.cell.2007.08.003
956 Lee, M., Kim, B., & Kim, V. N. (2014). Emerging roles of RNA modification: m(6)A and U-tail. *Cell*,
957 *158*(5), 980-987. https://doi.org/10.1016/j.cell.2014.08.005
958 Lence, T., Akhtar, J., Bayer, M., Schmid, K., Spindler, L., Ho, C. H., Kreim, N., Andrade-Navarro, M.
959 A., Poeck, B., Helm, M., & Roignant, J. Y. (2016). m(6)A modulates neuronal functions and sex
960 determination in *Drosophila*. *Nature*, *540*(7632), 242-247.
961 https://doi.org/10.1038/nature20568
962 Lence, T., Soller, M., & Roignant, J. Y. (2017). A fly view on the roles and mechanisms of the m(6)A
963 mRNA modification and its players. *RNA Biology*, *14*(9), 1232-1240.
964 https://doi.org/10.1080/15476286.2017.1307484
965 Letourneau, A., Santoni, F. A., Bonilla, X., Sailani, M. R., Gonzalez, D., Kind, J., Chevalier, C.,
966 Thurman, R., Sandstrom, R. S., Hibaoui, Y., Garieri, M., Popadin, K., Falconnet, E., Gagnebin,
967 M., Gehrig, C., Vannier, A., Guipponi, M., Farinelli, L., Robyr, D., . . . Antonarakis, S. E. (2014).
968 Domains of genome-wide gene expression dysregulation in Down's syndrome. *Nature*,
969 *508*(7496), 345-350. https://doi.org/10.1038/nature13200
970 Li, Y., Xia, L., Tan, K., Ye, X., Zuo, Z., Li, M., Xiao, R., Wang, Z., Liu, X., Deng, M., Cui, J., Yang, M., Luo,
971 Q., Liu, S., Cao, X., Zhu, H., Liu, T., Hu, J., Shi, J., . . . Xia, L. (2020). *N*6-Methyladenosine
972 co-transcriptionally directs the demethylation of histone H3K9me2. *Nature Genetics*.
973 https://doi.org/10.1038/s41588-020-0677-3
974 Liu, J., Gao, M., He, J., Wu, K., Lin, S., Jin, L., Chen, Y., Liu, H., Shi, J., Wang, X., Chang, L., Lin, Y.,
975 Zhao, Y. L., Zhang, X., Zhang, M., Luo, G. Z., Wu, G., Pei, D., Wang, J., . . . Chen, J. (2021). The
976 RNA m(6)A reader YTHDC1 silences retrotransposons and guards ES cell identity. *Nature*,
977 *591*(7849), 322-326. https://doi.org/10.1038/s41586-021-03313-9
978 Love, M. I., Huber, W., & Anders, S. (2014). Moderated estimation of fold change and dispersion
979 for RNA-seq data with DESeq2. *Genome Biology*, *15*(12), 550.
980 https://doi.org/10.1186/s13059-014-0550-8
981 Lucchesi, J. C. (2018). Transcriptional modulation of entire chromosomes: dosage compensation.
982 *Journal of Genetics*, *97*(2), 357-364. https://doi.org/10.1007/s12041-018-0919-7

983 Luo, G. Z., MacQueen, A., Zheng, G., Duan, H., Dore, L. C., Lu, Z., Liu, J., Chen, K., Jia, G., Bergelson,
984 J., & He, C. (2014). Unique features of the m6A methylome in *Arabidopsis thaliana*. *Nat*
985 *Commun*, *5*, 5630. https://doi.org/10.1038/ncomms6630
986 Ma, S., Chen, C., Ji, X., Liu, J., Zhou, Q., Wang, G., Yuan, W., Kan, Q., & Sun, Z. (2019). The interplay
987 between m6A RNA methylation and noncoding RNA in cancer. *Journal of Hematology &*
988 *Oncology*, *12*(1), 121. https://doi.org/10.1186/s13045-019-0805-7
989 Meng, J., Cui, X. D., Rao, M. K., Chen, Y. D., & Huang, Y. F. (2013). Exome-based analysis for RNA
990 epigenome sequencing data. *Bioinformatics*, *29*(12), 1565-1567.
991 https://doi.org/10.1093/bioinformatics/btt171
992 Meyer, K. D., & Jaffrey, S. R. (2014). The dynamic epitranscriptome: *N*6-methyladenosine and
993 gene expression control. *Nature Reviews: Molecular Cell Biology*, *15*(5), 313-326.
994 https://doi.org/10.1038/nrm3785
995 Meyer, K. D., Patil, D. P., Zhou, J., Zinoviev, A., Skabkin, M. A., Elemento, O., Pestova, T. V., Qian, S.
996 B., & Jaffrey, S. R. (2015). 5′ UTR m6A Promotes Cap-Independent Translation. *Cell*, *163*(4),
997 999-1010. https://doi.org/10.1016/j.cell.2015.10.012
998 Meyer, K. D., Saletore, Y., Zumbo, P., Elemento, O., Mason, C. E., & Jaffrey, S. R. (2012).
999 Comprehensive analysis of mRNA methylation reveals enrichment in 3' UTRs and near stop
1000 codons. *Cell*, *149*(7), 1635-1646. https://doi.org/10.1016/j.cell.2012.05.003
1001 Orr, B., Godek, K. M., & Compton, D. (2015). Aneuploidy. *Current Biology*, *25*(13), R538-R542.
1002 https://doi.org/10.1016/j.cub.2015.05.010
1003 Park, S. W., Oh, H., Lin, Y. R., & Park, Y. (2010). MSL *cis*-spreading from *roX* gene up-regulates the
1004 neighboring genes. *Biochem Biophys Res Commun*, *399*(2), 227-231.
1005 https://doi.org/10.1016/j.bbrc.2010.07.059
1006 Patil, D. P., Chen, C. K., Pickering, B. F., Chow, A., Jackson, C., Guttman, M., & Jaffrey, S. R. (2016).
1007 m(6)A RNA methylation promotes *XIST*-mediated transcriptional repression. *Nature*,
1008 *537*(7620), 369-373. https://doi.org/10.1038/nature19342
1009 Penn, J. K., Graham, P., Deshpande, G., Calhoun, G., Chaouki, A. S., Salz, H. K., & Schedl, P. (2008).
1010 Functioning of the *Drosophila* Wilms'-tumor-1-associated protein homolog, *Fl(2)d*, in
1011 *Sex-lethal*-dependent alternative splicing. *Genetics*, *178*(2), 737-748.
1012 https://doi.org/10.1534/genetics.107.081679

1013 Pertea, M., Pertea, G. M., Antonescu, C. M., Chang, T. C., Mendell, J. T., & Salzberg, S. L. (2015).
1014 StringTie enables improved reconstruction of a transcriptome from RNA-seq reads. *Nature*
1015 *Biotechnology*, *33*(3), 290-295. https://doi.org/10.1038/nbt.3122
1016 Pinello, N., Sun, S., & Wong, J. J. (2018). Aberrant expression of enzymes regulating m(6)A mRNA
1017 methylation: implication in cancer. *Cancer Biol Med*, *15*(4), 323-334.
1018 https://doi.org/10.20892/j.issn.2095-3941.2018.0365
1019 Prestel, M., Feller, C., & Becker, P. B. (2010). Dosage compensation and the global re-balancing of
1020 aneuploid genomes. *Genome Biology*, *11*(8), 216. https://doi.org/10.1186/gb-2010-11-8-216
1021 Rabinow, L., & Birchler, J. A. (1989). A dosage-sensitive modifier of retrotransposon-induced
1022 alleles of the *Drosophila white* locus. *EMBO Journal*, *8*(3), 879-889.
1023 https://www.ncbi.nlm.nih.gov/pubmed/2542025
1024 Raffel, G. D., Mercher, T., Shigematsu, H., Williams, I. R., Cullen, D. E., Akashi, K., Bernard, O. A., &
1025 Gilliland, D. G. (2007). *Ott1*(*Rbm15*) has pleiotropic roles in hematopoietic development.
1026 *Proceedings of the National Academy of Sciences of the United States of America*, *104*(14),
1027 6001-6006. https://doi.org/10.1073/pnas.0609041104
1028 Ramírez, F., Dündar, F., Diehl, S., Grüning, B. A., & Manke, T. (2014). deepTools: a flexible platform
1029 for exploring deep-sequencing data. *Nucleic Acids Research*, *42*(W1), W187-W191.
1030 https://doi.org/10.1093/nar/gku365
1031 Raznahan, A., Parikshak, N. N., Chandran, V., Blumenthal, J. D., Clasen, L. S., Alexander-Bloch, A. F.,
1032 Zinn, A. R., Wangsa, D., Wise, J., Murphy, D. G. M., Bolton, P. F., Ried, T., Ross, J., Giedd, J. N., &
1033 Geschwind, D. H. (2018). Sex-chromosome dosage effects on gene expression in humans.
1034 *Proceedings of the National Academy of Sciences of the United States of America*, *115*(28),
1035 7398-7403. https://doi.org/10.1073/pnas.1802889115
1036 Roseman, R. R., Pirrotta, V., & Geyer, P. K. (1993). The *su(Hw)* protein insulates expression of the
1037 *Drosophila melanogaster white* gene from chromosomal position-effects. *EMBO Journal*,
1038 *12*(2), 435-442. https://doi.org/DOI 10.1002/j.1460-2075.1993.tb05675.x
1039 Roundtree, I. A., Evans, M. E., Pan, T., & He, C. (2017a). Dynamic RNA Modifications in Gene
1040 Expression Regulation. *Cell*, *169*(7), 1187-1200. https://doi.org/10.1016/j.cell.2017.05.045
1041 Roundtree, I. A., Luo, G. Z., Zhang, Z. J., Wang, X., Zhou, T., Cui, Y. Q., Sha, J. H., Huang, X. X.,
1042 Guerrero, L., Xie, P., He, E., Shen, B., & He, C. (2017b). YTHDC1 mediates nuclear export of

1043 *N*6-methyladenosine methylated mRNAs. *Elife*, *6*, e31311. https://doi.org/ARTN e31311
1044 Rücklé, C., Körtel, N., Basilicata, M. F., Busch, A., Zhou, Y., Hoch-Kraft, P., Tretow, K., Kielisch, F.,
1045 Bertin, M., Pradhan, M., Musheev, M., Schweiger, S., Niehrs, C., Rausch, O., Zarnack, K.,
1046 Valsecchi, C. I. K., & König, J. (2023). RNA stability controlled by m(6)A methylation
1047 contributes to X-to-autosome dosage compensation in mammals. *Nature Structural &*
1048 *Molecular Biology*, *30*(8). https://doi.org/10.1038/s41594-023-00997-7
1049 San Roman, A. K., Godfrey, A. K., Skaletsky, H., Bellott, D. W., Groff, A. F., Harris, H. L., Blanton, L.
1050 V., Hughes, J. F., Brown, L., Phou, S., Buscetta, A., Kruszka, P., Banks, N., Dutra, A., Pak, E.,
1051 Lasutschinkow, P. C., Keen, C., Davis, S. M., Tartaglia, N. R., . . . Page, D. C. (2023). The human
1052 inactive X chromosome modulates expression of the active X chromosome. *Cell Genom*, *3*(2),
1053 100259. https://doi.org/10.1016/j.xgen.2023.100259
1054 Sanchez-Pavon, E., Mendoza, H., & Garcia-Ferreyra, J. (2021). Trisomy 21 and Assisted
1055 Reproductive Technologies: A review. *JBRA Assist Reprod*, *26*(1), 129-141.
1056 https://doi.org/10.5935/1518-0557.20210047
1057 Schindelin, J., Arganda-Carreras, I., Frise, E., Kaynig, V., Longair, M., Pietzsch, T., Preibisch, S.,
1058 Rueden, C., Saalfeld, S., Schmid, B., Tinevez, J. Y., White, D. J., Hartenstein, V., Eliceiri, K.,
1059 Tomancak, P., & Cardona, A. (2012). Fiji: an open-source platform for biological-image analysis.
1060 *Nature Methods*, *9*(7), 676-682. https://doi.org/10.1038/Nmeth.2019
1061 Shafik, A. M., Zhang, F., Guo, Z., Dai, Q., Pajdzik, K., Li, Y., Kang, Y., Yao, B., Wu, H., He, C., Allen, E.
1062 G., Duan, R., & Jin, P. (2021). *N*6-methyladenosine dynamics in neurodevelopment and aging,
1063 and its potential role in Alzheimer's disease. *Genome Biology*, *22*(1), 17.
1064 https://doi.org/10.1186/s13059-020-02249-z
1065 Shen, S. H., Park, J. W., Lu, Z. X., Lin, L., Henry, M. D., Wu, Y. N., Zhou, Q., & Xing, Y. (2014). rMATS:
1066 Robust and flexible detection of differential alternative splicing from replicate RNA-Seq data.
1067 *Proceedings of the National Academy of Sciences of the United States of America*, *111*(51),
1068 E5593-E5601. https://doi.org/10.1073/pnas.1419161111
1069 Shi, X., Yang, H., Chen, C., Hou, J., Hanson, K. M., Albert, P. S., Ji, T., Cheng, J., & Birchler, J. A.
1070 (2021). Genomic imbalance determines positive and negative modulation of gene expression
1071 in diploid maize. *Plant Cell*, *33*(4), 917-939. https://doi.org/10.1093/plcell/koab030
1072 Shi, X., Yang, H., Chen, C., Hou, J., Ji, T., Cheng, J., & Birchler, J. A. (2022). Dosage-sensitive miRNAs

1073 trigger modulation of gene expression during genomic imbalance in maize. *Nat Commun*,
1074 *13*(1), 3014. https://doi.org/10.1038/s41467-022-30704-x
1075 Stark, R., Brown, G. (2013). DiffBind: differential binding analysis of ChIP-seq peak data.
1076 *Bioconductor package*. http://www.bioconductor.org. DOI: 10.18129/B9.bioc.DiffBind.
1077 Sun, L., Fernandez, H. R., Donohue, R. C., Li, J., Cheng, J., & Birchler, J. A. (2013a). Male-specific
1078 lethal complex in *Drosophila* counteracts histone acetylation and does not mediate dosage
1079 compensation. *Proceedings of the National Academy of Sciences of the United States of*
1080 *America*, *110*(9), E808-E817. https://doi.org/10.1073/pnas.1222542110
1081 Sun, L., Johnson, A. F., Donohue, R. C., Li, J., Cheng, J., & Birchler, J. A. (2013b). Dosage
1082 compensation and inverse effects in triple X metafemales of *Drosophila*. *Proceedings of the*
1083 *National Academy of Sciences of the United States of America*, *110*(18), 7383-7388.
1084 https://doi.org/10.1073/pnas.1305638110
1085 Sun, L., Johnson, A. F., Li, J., Lambdin, A. S., Cheng, J., & Birchler, J. A. (2013c). Differential effect of
1086 aneuploidy on the X chromosome and genes with sex-biased expression in *Drosophila*.
1087 *Proceedings of the National Academy of Sciences of the United States of America*, *110*(41),
1088 16514-16519. https://doi.org/10.1073/pnas.1316041110
1089 Szklarczyk, D., Gable, A. L., Lyon, D., Junge, A., Wyder, S., Huerta-Cepas, J., Simonovic, M.,
1090 Doncheva, N. T., Morris, J. H., Bork, P., Jensen, L. J., & Mering, C. (2019). STRING v11:
1091 protein-protein association networks with increased coverage, supporting functional
1092 discovery in genome-wide experimental datasets. *Nucleic Acids Research*, *47*(D1), D607-D613.
1093 https://doi.org/10.1093/nar/gky1131
1094 Thorvaldsdóttir, H., Robinson, J. T., & Mesirov, J. P. (2013). Integrative Genomics Viewer (IGV):
1095 high-performance genomics data visualization and exploration. *Briefings in Bioinformatics*,
1096 *14*(2), 178-192. https://doi.org/10.1093/bib/bbs017
1097 Villanueva, R. A. M., & Chen, Z. J. (2019). ggplot2: Elegant Graphics for Data Analysis, 2nd edition.
1098 *Measurement-Interdisciplinary Research and Perspectives*, *17*(3), 160-167.
1099 https://doi.org/10.1080/15366367.2019.1565254
1100 Wang, X., Lu, Z. K., Gomez, A., Hon, G. C., Yue, Y. N., Han, D. L., Fu, Y., Parisien, M., Dai, Q., Jia, G.
1101 F., Ren, B., Pan, T., & He, C. (2014). *N*6-methyladenosine-dependent regulation of messenger
1102 RNA stability. *Nature*, *505*(7481), 117-120. https://doi.org/10.1038/nature12730

1103 Wang, Y., Li, Y., Toth, J. I., Petroski, M. D., Zhang, Z., & Zhao, J. C. (2014). *N*6-methyladenosine
1104 modification destabilizes developmental regulators in embryonic stem cells. *Nature Cell*
1105 *Biology*, *16*(2), 191-198. https://doi.org/10.1038/ncb2902
1106 Wang, Y., Li, Y., Yue, M. H., Wang, J., Kumar, S., Wechsler-Reya, R. J., Zhang, Z. L., Ogawa, Y., Kellis,
1107 M., Duester, G., & Zhao, J. C. (2018). N(6)-methyladenosine RNA modification regulates
1108 embryonic neural stem cell self-renewal through histone modifications. *Nature Neuroscience*,
1109 *21*(8), 1139-1139. https://doi.org/10.1038/s41593-018-0169-2
1110 Williams, B. R., Prabhu, V. R., Hunter, K. E., Glazier, C. M., Whittaker, C. A., Housman, D. E., &
1111 Amon, A. (2008). Aneuploidy affects proliferation and spontaneous immortalization in
1112 mammalian cells. *Science*, *322*(5902), 703-709. https://doi.org/10.1126/science.1160058
1113 Wu, T., Hu, E., Xu, S., Chen, M., Guo, P., Dai, Z., Feng, T., Zhou, L., Tang, W., Zhan, L., Fu, X., Liu, S.,
1114 Bo, X., & Yu, G. (2021). clusterProfiler 4.0: A universal enrichment tool for interpreting omics
1115 data. *Innovation (N Y)*, *2*(3), 100141. https://doi.org/10.1016/j.xinn.2021.100141
1116 Xie, W., & Birchler, J. A. (2012). Identification of Inverse Regulator-a (*Inr-a*) as Synonymous with
1117 Pre-mRNA Cleavage Complex II Protein (*Pcf11*) in *Drosophila*. *G3 (Bethesda)*, *2*(6), 701-706.
1118 https://doi.org/10.1534/g3.112.002071
1119 Yan, D., & Perrimon, N. (2015). *spenito* is required for sex determination in *Drosophila*
1120 *melanogaster*. *Proceedings of the National Academy of Sciences of the United States of*
1121 *America*, *112*(37), 11606-11611. https://doi.org/10.1073/pnas.1515891112
1122 Yang, H., Shi, X., Chen, C., Hou, J., Ji, T., Cheng, J., & Birchler, J. A. (2021). Predominantly inverse
1123 modulation of gene expression in genomically unbalanced disomic haploid maize. *Plant Cell*,
1124 *33*(4), 901-916. https://doi.org/10.1093/plcell/koab029
1125 Yang, Y., Hsu, P. J., Chen, Y. S., & Yang, Y. G. (2018). Dynamic transcriptomic m(6)A decoration:
1126 writers, erasers, readers and functions in RNA metabolism. *Cell Research*, *28*(6), 616-624.
1127 https://doi.org/10.1038/s41422-018-0040-8
1128 Yu, G. C., Wang, L. G., & He, Q. Y. (2015). ChIPseeker: an R/Bioconductor package for ChIP peak
1129 annotation, comparison and visualization. *Bioinformatics*, *31*(14), 2382-2383.
1130 https://doi.org/10.1093/bioinformatics/btv145
1131 Zaccara, S., Ries, R. J., & Jaffrey, S. R. (2019). Reading, writing and erasing mRNA methylation.
1132 *Nature Reviews: Molecular Cell Biology*, *20*(10), 608-624.

https://doi.org/10.1038/s41580-019-0168-5

Zhang, L. D., Zhang, S., Wang, R. X., & Sun, L. (2022). Genome-Wide Identification of Long Noncoding RNA and Their Potential Interactors in *ISWI* Mutants. *International Journal of Molecular Sciences*, *23*(11), 6247. https://doi.org/10.3390/ijms23116247

Zhang, S., Qi, H., Huang, C., Yuan, L., Zhang, L., Wang, R., Tian, Y., & Sun, L. (2021a). Interaction of Male Specific Lethal complex and genomic imbalance on global gene expression in *Drosophila*. *Scientific Reports*, *11*(1), 19679. https://doi.org/10.1038/s41598-021-99268-y

Zhang, S., Wang, R., Huang, C., Zhang, L., & Sun, L. (2021b). Modulation of Global Gene Expression by Aneuploidy and CNV of Dosage Sensitive Regulatory Genes. *Genes (Basel)*, *12*(10), 1606. https://doi.org/10.3390/genes12101606

Zhang, S., Wang, R., Zhu, X., Zhang, L., Liu, X., & Sun, L. (2023). Characteristics and expression of lncRNA and transposable elements in *Drosophila* aneuploidy. *iScience*, *26*(12), 108494. https://doi.org/10.1016/j.isci.2023.108494

Zhao, B. S., Wang, X., Beadell, A. V., Lu, Z., Shi, H., Kuuspalu, A., Ho, R. K., & He, C. (2017). m(6)A-dependent maternal mRNA clearance facilitates zebrafish maternal-to-zygotic transition. *Nature*, *542*(7642), 475-478. https://doi.org/10.1038/nature21355

Zhong, S. L., Li, H. Y., Bodi, Z., Button, J., Vespa, L., Herzog, M., & Fray, R. G. (2008). MTA is an messenger RNA adenosine methylase and interacts with a homolog of a sex-specific splicing factor. *Plant Cell*, *20*(5), 1278-1288. https://doi.org/10.1105/tpc.108.058883

Zhu, C., Zhang, S., Zhou, C., Tian, C., Shi, B., Xu, K., Huang, L., Sun, Y., Lin, Y., Lai, Z., & Guo, Y. (2023). RNA Methylome Reveals the m(6)A-mediated Regulation of Flavor Metabolites in Tea Leaves under Solar-withering. *Genomics Proteomics Bioinformatics*, *21*(4), 769-787. https://doi.org/10.1016/j.gpb.2023.02.003

Figures

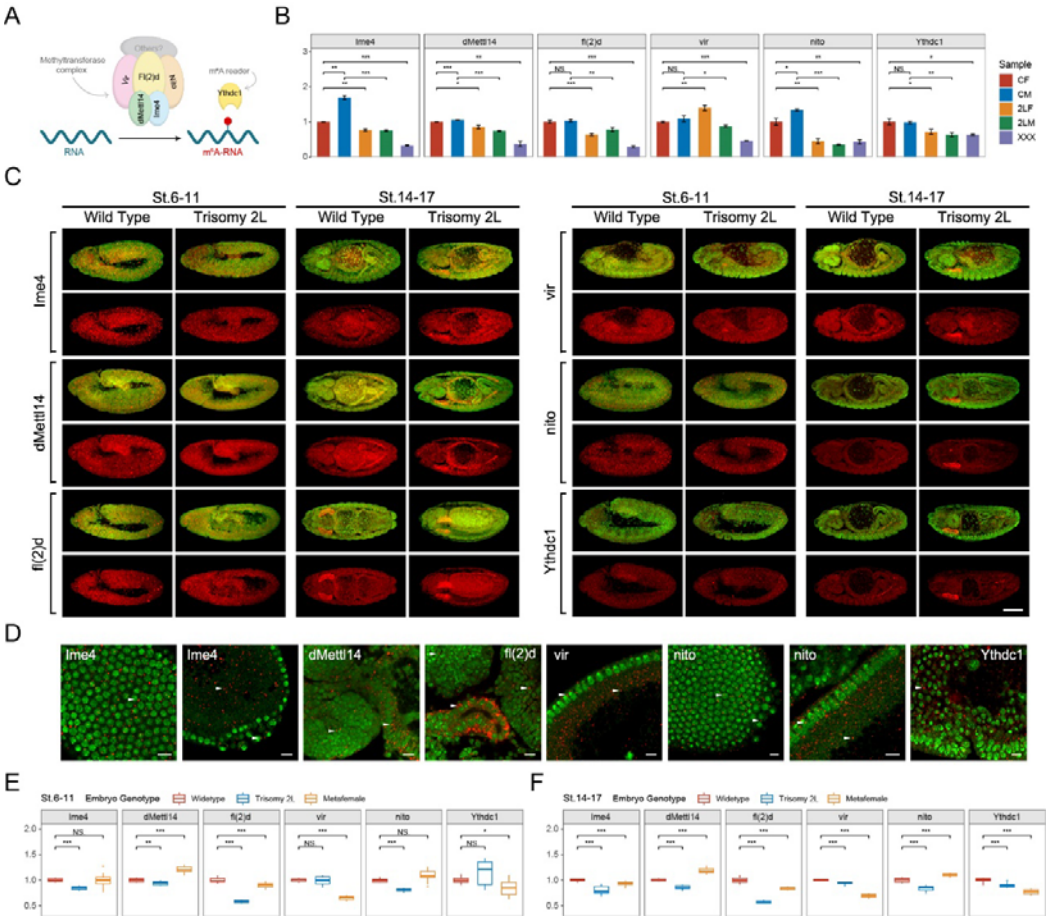

Figure 1. The responses of m^{6}A methyltransferases and reader protein under the condition of genomic imbalance. (**A**) Schematic diagram of m^{6}A components in *Drosophila*. (**B**) RT-qPCR analysis of mRNA levels of m^{6}A methyltransferases and reader protein in third instar larvae of wildtype and trisomy *Drosophila*. CF, wildtype female control; CM, wildtype male control; 2LF, trisomy 2L female; 2LM, trisomy 2L male; XXX, metafemale; 2L, chromosome 2 left arm. Student's *t* test *p < 0.05, **p < 0.01, ***p < 0.001. (**C**) Subembryonic distribution patterns of the transcripts of m^{6}A components in wildtype and trisomy 2L *Drosophila*. The names of the genes were shown in the left of the pictures; the genotypes and stages were shown above. Red, probes; green, DAPI. Scale bar, 100 µm. (**D**) Subcellular localization of probe signals. Probe name was written in the corner of each picture. Red, probe; green, DAPI. Arrowheads indicate the foci of probe signals. The tissue types are (1) blastoderm nuclei; (2) yolk plasm and pole cells; (3) brain and midgut; (4) salivary gland and midgut; (5) blastoderm nuclei and yolk cortex; (6) blastoderm nuclei and pole cells; (7) blastoderm nuclei and yolk cortex; (8) germ band. Scale bars, 10 µm. (**E**,**F**) The expression levels of m^{6}A component genes in stage 6-11 (**E**) and stage 14-17 (**F**) represented

by relative fluorescence intensity of probes compared with DAPI signals. The expression of wildtype embryos was set as one. Sample size = 10. Student's *t* test *p < 0.05, **p < 0.01, ***p < 0.001.

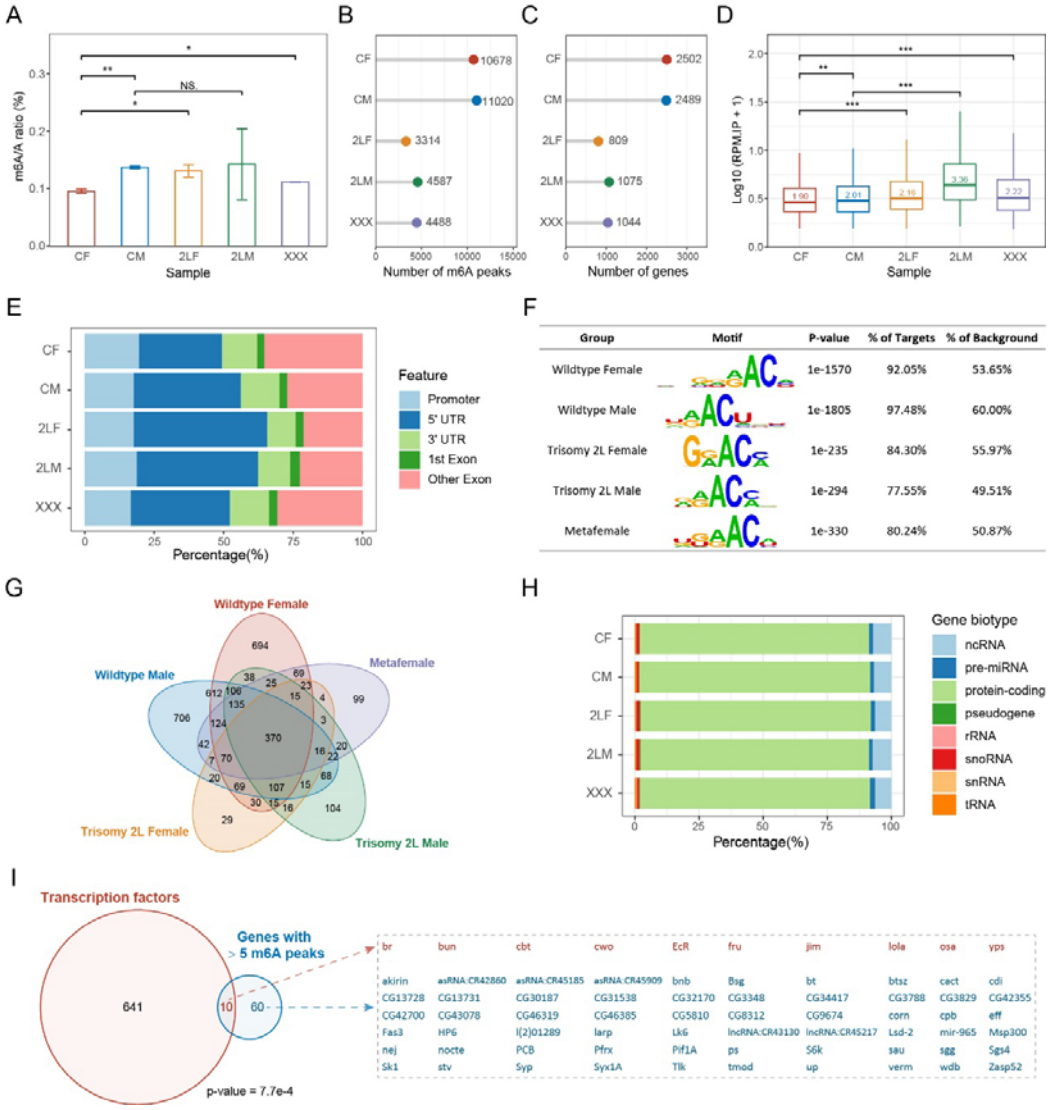

Figure 2. Overview of RNA m^{6}A methylation in aneuploid *Drosophila*. (**A**) Global m^{6}A abundance in third instar larvae of wildtype and aneuploid *Drosophila*. Data represent the mean of two independent experiments, each containing three or four biological replicates. Quantification was performed using EpiQuik m^{6}A RNA Methylation Quantification Kit. Error bar indicates the standard error of the means (SEM). Student's *t* test *p < 0.05, **p < 0.01. (**B**) The number of m^{6}A peaks identified by MeRIP-Seq. (**C**) The number of m^{6}A-modified genes obtained by annotating

1186 the peaks. (**D**) Expression levels of m^6A modification sites in IP samples expressed as
1187 log10-transformed reads per million (RPM). The number on the boxplot indicates the median
1188 RPM of each sample. Mann-Whitney U test *p < 0.05, **p < 0.01, ***p < 0.001. (**E**) Percentages
1189 of peaks localized on different gene features. (**F**) The most enriched motifs obtained by *de novo*
1190 motif analysis of the m^6A peaks. (**G**) Venn diagram showing the intersection of m^6A-modified
1191 genes in each sample. (**H**) Gene biotypes of m^6A-modified genes. (**I**) Venn diagram showing the
1192 intersection of transcription factors and m^6A-modified genes with more than five m^6A peaks in all
1193 samples. Seventy genes with more than five m^6A peaks were listed on the right, with
1194 transcription factors in red and others in blue. P-value indicates one-tailed Fisher's exact test. CF,
1195 wildtype female control; CM, wildtype male control; 2LF, trisomy 2L female; 2LM, trisomy 2L male;
1196 XXX, metafemale; 5′UTR, 5′ untranslated region; 3′UTR, 3′ untranslated region; MeRIP-Seq,
1197 m^6A methylated RNA immunoprecipitation sequencing.
1198

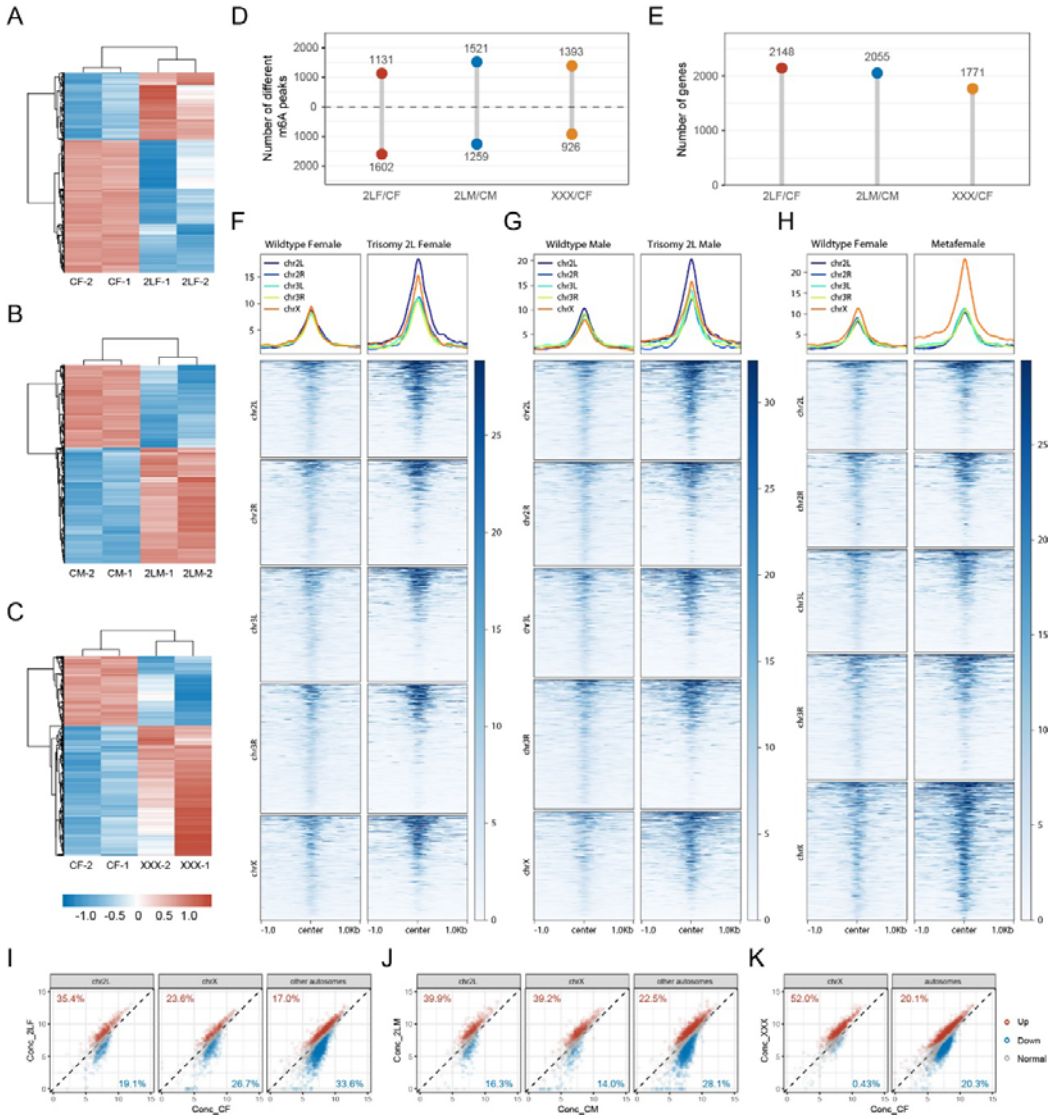

Figure 3. Differential m^{6}A methylome analysis of aneuploid *Drosophila*. (**A-C**) Heatmaps of differentially methylated peaks (DMPs) in trisomy 2L females (**A**), trisomy 2L males (**B**) and metafemales (**C**), and their corresponding control groups. The threshold of significance was p-value ≤ 0.1. (**D**) The number of DMPs. The threshold of significance was set to p-value ≤ 0.1. The numbers above the horizontal dashed lines indicate peaks with upregulated methylation levels, and the numbers below indicate peaks with downregulated methylation levels. (**E**) The number of DMP-associated genes. (**F-H**) Profiles and heatmaps illustrating the density of m^{6}A-modified reads at the DMP positions in trisomy 2L females (**F**), trisomy 2L males (**G**), metafemales (**H**), and their corresponding controls. The DMPs were divided into five groups according to the chromosomes they located. (**I-K**) Scatter plots showing the concentration of

reads at methylation sites on different chromosomes in trisomy 2L females (**I**), trisomy 2L males (**J**), and metafemales (**K**). Red points indicate significantly up-regulated m^6A peaks, blue points indicate significantly down-regulated m^6A peaks, and gray points indicate m^6A peaks without significant changes. The percentages of DMPs on *cis* and *trans* chromosomes were indicated in the corners of the plots. CF, wildtype female control; CM, wildtype male control; 2LF, trisomy 2L female; 2LM, trisomy 2L male; XXX, metafemale.

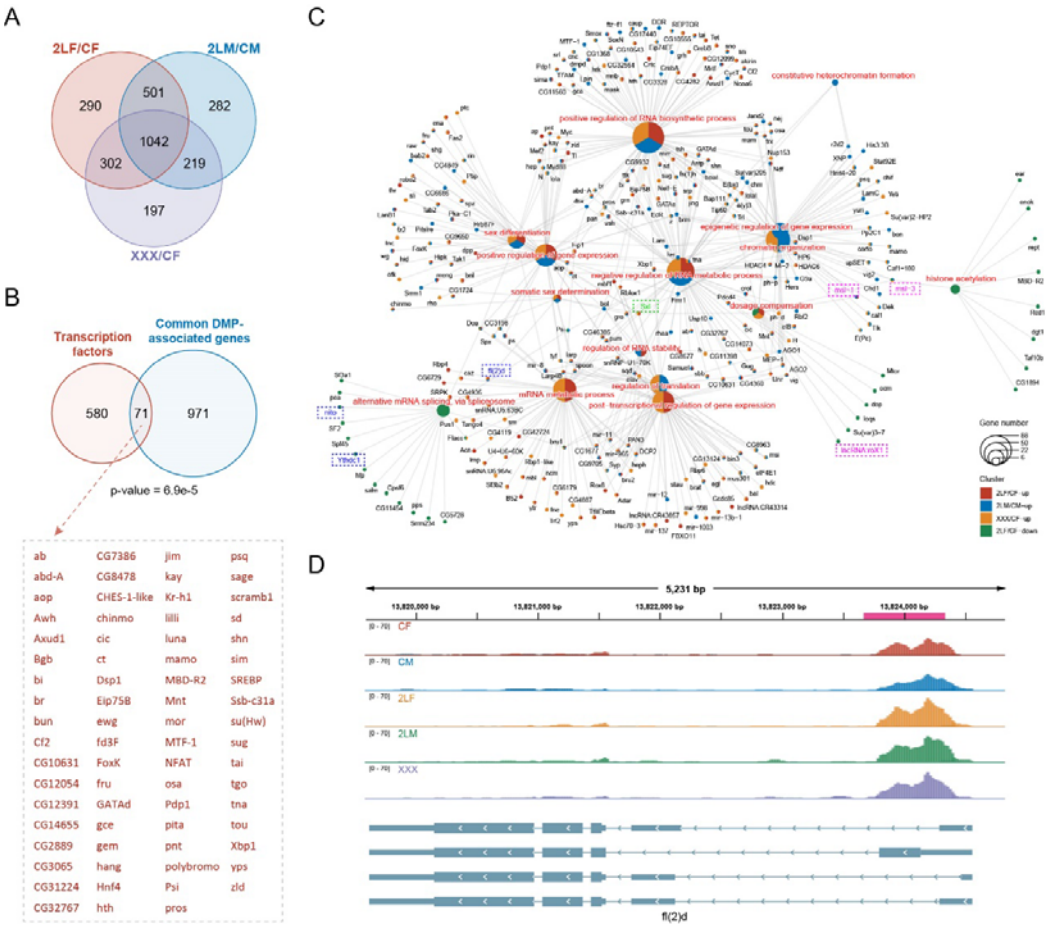

Figure 4. Differentially methylated peak (DMP) associated genes and their functions. (A) Venn diagram showing the number of common DMP-associated genes in three types of aneuploidies compared with wildtypes. (B) Venn diagram showing the intersection of transcription factors and the common DMP-associated genes in all comparisons. Transcription factors with DMPs were listed on the right. P-value indicates one-tailed Fisher's exact test. (C) Network showing the functions related to expression regulation and dosage compensation enriched by DMP-associated genes. The color of the nodes indicates the comparison, and the size of the function nodes

1225 represents the number of DMP-associated genes connected with them. (D) Genome browser

1226 example of *fl(2)d* for indicated MeRIP-seq data. Steelblue color represents input reads, while

1227 other colors represent IP reads. Signals were displayed as the mean CPM of two biological

1228 replicates. The gene architectures were shown at the bottom. The magenta rectangles at above

1229 represent differentially methylated peak. CF, wildtype female control; CM, wildtype male control;

1230 2LF, trisomy 2L female; 2LM, trisomy 2L male; XXX, metafemale.

1231

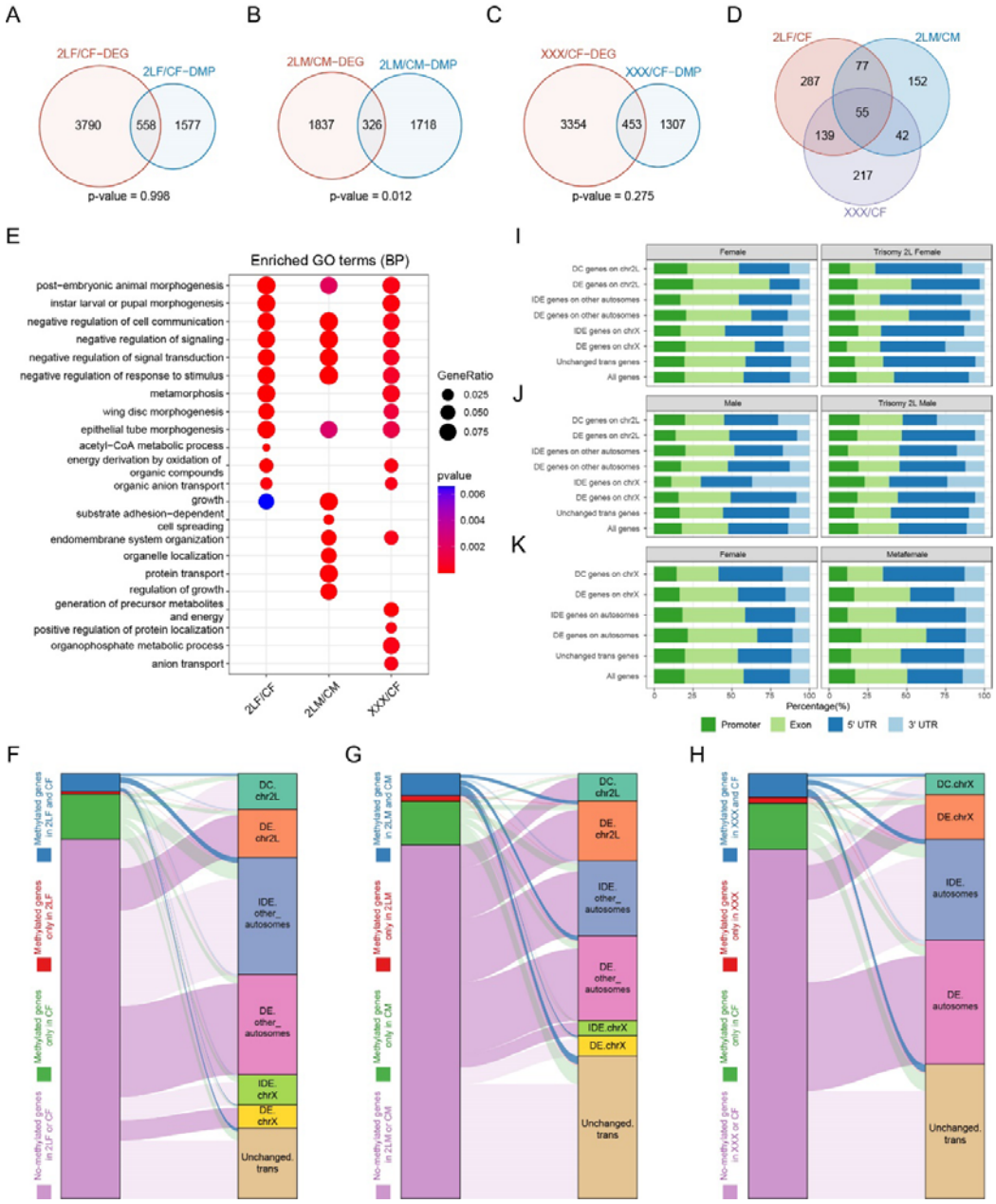

1232

1233 **Figure 5.** Relationships between RNA m^{6}A methylation and gene expression in aneuploidy. (**A-C**)

1234 Venn diagrams showing the intersections of differentially expressed genes (DEGs) and
1235 differentially methylated peak (DMP) associated genes in trisomy 2L females (**A**), trisomy 2L
1236 males (**B**), and metafemales (**C**) compared with their corresponding controls. P-values indicate
1237 one-tailed Fisher's exact tests. (**D**) The common differentially expressed and differentially
1238 methylated genes in all groups. (**E**) Functional enrichment analysis of simultaneously differentially
1239 expressed and differentially methylated genes. Top 10 enriched GO terms (Biological Process)
1240 with p-value < 0.1 in each comparison were shown. (**F-H**) Sankey diagrams showing the
1241 relationships between genes with different m^6A-modified states and genes with canonical dosage
1242 effect (DE), dosage compensation (DC), and inverse dosage effect (IDE) in trisomy 2L females (**F**),
1243 trisomy 2L males (**G**), and metafemales (**H**). Enrichment analysis was performed on each two
1244 groups of genes, and deep color lines indicate significant connection relationships (Fisher's exact
1245 test p-value < 0.05). (**I-K**) Gene feature distributions for m^6A peaks on genes with canonical DE,
1246 DC, and IDE in trisomy 2L females (**I**), trisomy 2L males (**J**), metafemales (**K**), and their
1247 corresponding controls. CF, wildtype female control; CM, wildtype male control; 2LF, trisomy 2L
1248 female; 2LM, trisomy 2L male; XXX, metafemale; DEG, differentially expressed gene; DMP,
1249 differentially methylated peak; DE, dosage effect; DC, dosage compensation; IDE, inverse dosage
1250 effect. Canonical DE refers to ratio > 1.25, DC stands for 0.8 < ratio < 1.25, IDE stands for 0.5 <
1251 ratio < 0.8, and unchanged refers to 0.8 < ratio < 1.25.
1252

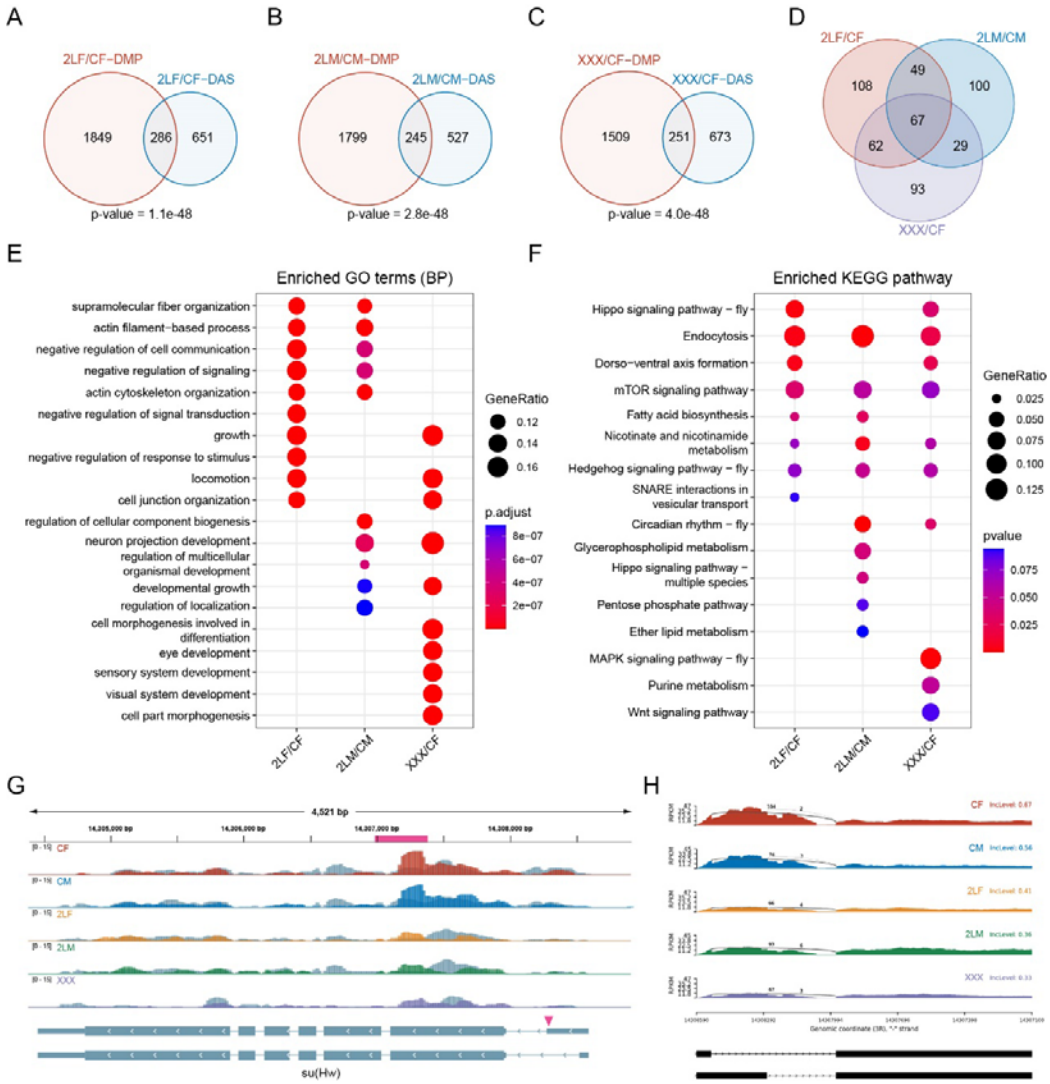

Figure 6. Combined analysis of differential alternative splicing and differential methylation. (**A-C**) Venn diagrams showing the intersections of differential alternative splicing (DAS) genes and differentially methylated peak (DMP) associated genes in trisomy 2L females (**A**), trisomy 2L males (**B**), and metafemales (**C**) compared with their corresponding controls. P-values indicate one-tailed Fisher's exact tests. (**D**) The common differentially alternatively spliced and differentially methylated genes in all groups. (**E**) Functional enrichment analysis of simultaneously differentially alternatively spliced and differentially methylated genes. Top 10 enriched GO terms (Biological Process) with p-value < 0.05 in each comparison were shown. (**F**) KEGG pathway enrichment analysis of simultaneously differentially alternatively spliced and differentially methylated genes. Top 10 enriched pathways with p-value < 0.1 in each comparison were shown. (**G**) Genome browser example of *su(Hw)* for indicated MeRIP-Seq data. Steelblue color represents

1265 input reads, while other colors represent IP reads. Signals were displayed as the mean CPM of
1266 two biological replicates. The gene architecture was shown at the bottom (only two
1267 representative transcript isoforms were shown). The magenta rectangle at above represents DMP.
1268 The magenta arrowhead indicates the position of differential alternative splicing. (**H**) Sashimi plot
1269 depicting RNA sequencing reads and exon junction reads at the position where the differential
1270 splicing events occurs on *su(Hw)*. The gene model was shown below. One of the biological
1271 replicates was chosen for representation. CF, wildtype female control; CM, wildtype male control;
1272 2LF, trisomy 2L female; 2LM, trisomy 2L male; XXX, metafemale; DAS, differential alternative
1273 splicing; DMP, differentially methylated peak; CPM, Counts per million; RPKM, Reads per kilobase
1274 per million mapped reads.
1275
1276

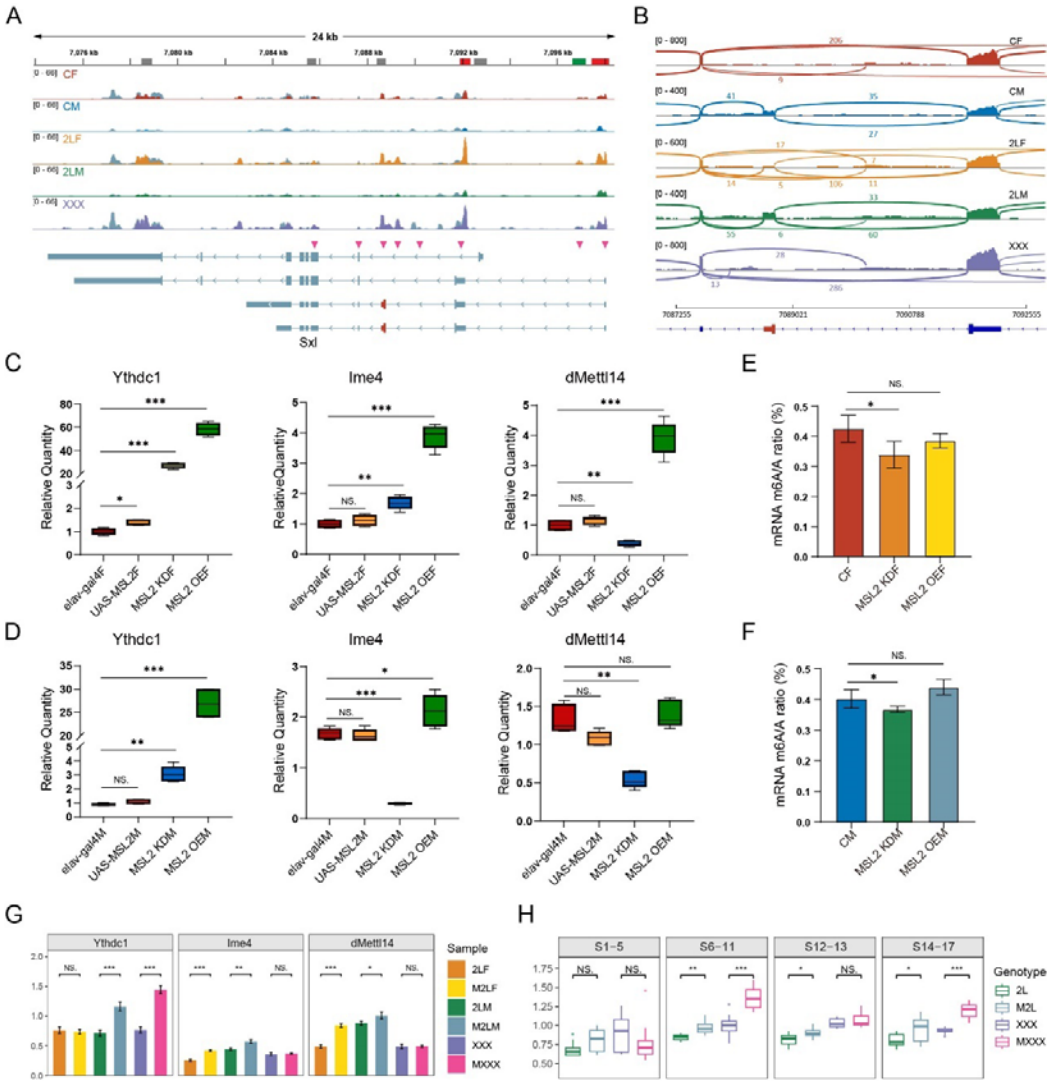

Figure 7. Interactions between m^{6}A and *Drosophila* Male Specific Lethal (MSL) complex. (**A**) Genome browser example of *Sxl* for indicated MeRIP-Seq data. Steelblue color represents input reads, while other colors represent IP reads. Signals were displayed as the mean CPM of two biological replicates. The gene architecture was shown at the bottom (only four representative transcript isoforms were shown). The rectangles at above represent m^{6}A peaks, where red indicates up-regulated DMPs, green indicates down-regulated DMP, and gray indicates no significant changes. The magenta arrowheads indicate the positions of alternative splicing. (**B**) Sashimi plot depicting RNA sequencing reads and exon junction reads at the position where the differential splicing events occurs on *Sxl*. The gene model was shown below, with the third exon indicated in red. One of the biological replicates was chosen for representation. CF, wildtype female control; CM, wildtype male control; 2LF, trisomy 2L female; 2LM, trisomy 2L male; XXX,

1289 metafemale. (**C**,**D**) RT-qPCR analysis of mRNA levels of m^6A components in the heads of MSL2
1290 transgenic female (**C**) and male (**D**) *Drosophila* adults. (**E**,**F**) Abundance of mRNA m^6A
1291 modification in the heads of MSL2 transgenic females (**E**) and males (**F**). Student's *t* test *p < 0.05,
1292 **p < 0.01, ***p < 0.001. MSL2 KDF, MSL2 neural-knockdown female; MSL2 KDM, MSL2
1293 neural-knockdown male; MSL2 OEF, MSL2-overexpressed female; MSL2 OEM,
1294 MSL2-overexpressed male. (**G**) RT-qPCR analysis of mRNA levels of m^6A regulators in the brains of
1295 trisomy and MSL2-overexpressed trisomy *Drosophila* larvae. Student's *t* test *p < 0.05, **p < 0.01,
1296 ***p < 0.001. 2LF, trisomy 2L female; 2LM, trisomy 2L male; XXX, metafemale; M2LF,
1297 MSL2-overexpressed trisomy 2L female; M2LM, MSL2-overexpressed trisomy 2L male; MXXX,
1298 MSL2-overexpressed metafemale. (**H**) The expression levels of Ime4 in trisomy and
1299 MSL2-overexpressed trisomy embryos represented by relative fluorescence intensity of probes.
1300 The expression of wildtype embryos was set as one. Sample size = 10. Student's *t* test *p < 0.05,
1301 **p < 0.01, ***p < 0.001. 2L, trisomy 2L; M2L, MSL2-overexpressed trisomy 2L; XXX, metafemale;
1302 MXXX, MSL2-overexpressed metafemale.
1303
1304

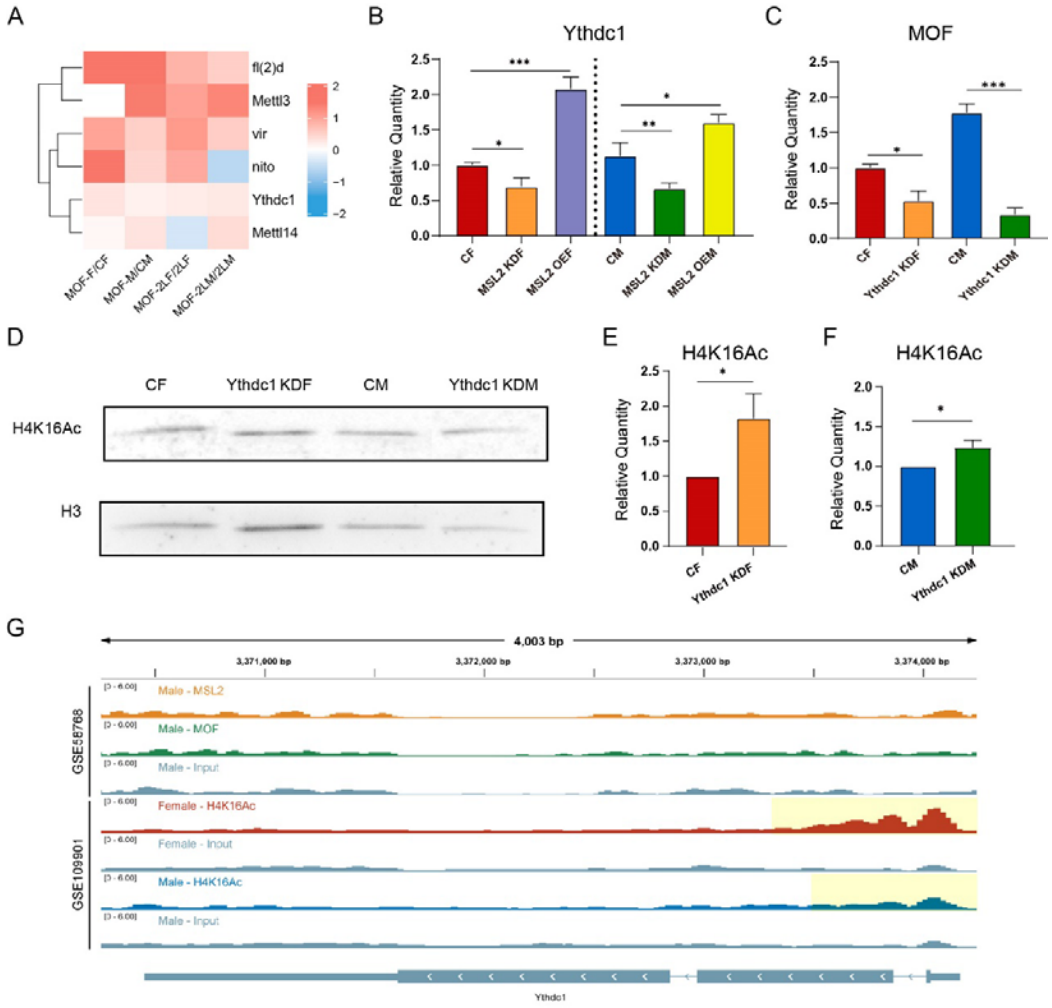

Figure 8. RNA m^{6}A modification regulate histone acetyltransferase MOF and H4K16Ac. (**A**) Heatmap of the expression changes of m^{6}A regulators in MOF overexpressing *Drosophila* larvae. The color of the heatmap represents log2(ratio). CF, wildtype female control; CM, wildtype male control; MOF-F, MOF-overexpressed female; MOF-M, MOF-overexpressed male; 2LF, trisomy 2L female; 2LM, trisomy 2L male; MOF-2LF, MOF-overexpressed trisomy 2L female; MOF-2LM, MOF-overexpressed trisomy 2L male. (**B**) RT-qPCR analysis of mRNA levels of *Ythdc1* in the heads of MSL2 transgenic *Drosophila*. MOF KDF, MOF neural-knockdown female; MOF KDM, MOF neural-knockdown male; MOF OEF, MOF-overexpressed female; MOF OEM, MOF-overexpressed male (**C**) RT-qPCR analysis of mRNA levels of MOF in the heads of *Ythdc1* knockdown *Drosophila*. Ythdc1 KDF, Ythdc1 neural-knockdown female; Ythdc1 KDM, Ythdc1 neural-knockdown male. (**D**) Western blot analysis of H4K16Ac in *Drosophila*. (**E**,**F**) Relative quantification of H4K16Ac in wild type and *Ythdc1* knockdown adult *Drosophila* based on western blot (N = 5). Ythdc1 KDF,

1318 Ythdc1-knockdown female; Ythdc1 KDM, Ythdc1-knockdown male. (**G**) Genome browser example

1319 of *Ythdc1* for indicated ChIP-seq data. Signals were displayed as CPM values. The gene

1320 architecture was shown at the bottom (only one representative transcript isoform was shown).

1321 The yellow shaded area indicates the presence of the H4K16Ac peaks..

1322

1323

1324 ## Figure supplements

1325

A

Primer	Sequence	Length
Ime4-L	CAAGTACGTGCACTATGAGG	159
Ime4-R	GTCATGTCCAAGAAGCGTAG	
dMettl14-L	GCCTCTTCCTCCAAGAAAAC	189
dMettl14-R	CCTCAACTTGGGATACTCCT	
fl(2)d-L	CCTGGACGTTATTTCCTACT	245
fl(2)d-R	TAAGCTAGAGACCATTCACG	
vir-L	GTACATGAAACCCTTAGAGGC	154
vir-R	CTTGCTTATGGAGAGATAGCG	
nito-L	GCCAGTACGGTTCCAGATGT	104
nito-R	CCGTCCGTCAAATGAAACTT	
Ythdc1-L	GGTCGTGATTTGATCCTCTG	153
Ythdc1-R	TCGAACTCACTCCCATACTC	
tubulin-F	AGCTCAGCACCCTCTGTGTAAT	208
tubulin-R	AGCTGGAGCGCATCAATGTGTA	

B

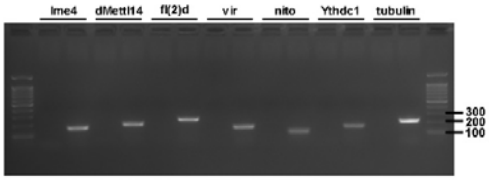

C

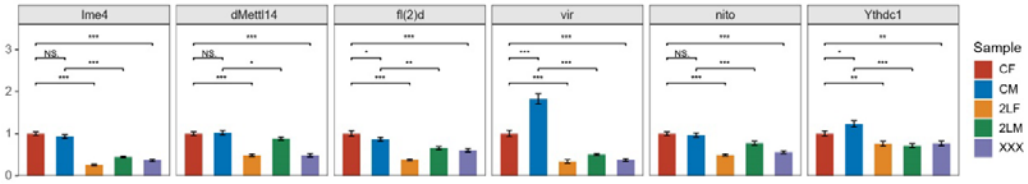

D

Primer	Sequence	Length
Ime4-F-T3	TGTTGGGAAATCACTCCCAATTAAGAGAAGTTTAAGTCCCACGG	1126
Ime4-R-T7	GTAATACGACTCACTATAGGGAGACCACCATCTGGATAACGCTTCTGG	
dMettl14-F-T3	TGTTGGGAAATCACTCCCAATTAACCAATCCGCACAATGACTAC	752
dMettl14-R-T7	GTAATACGACTCACTATAGGGAGACCACTAGCCAACCTGGTCGAATAC	
fl(2)d-F-T3	TGTTGGGAAATCACTCCCAATTAACTAGAGACCATTCACGAGGA	829
fl(2)d-R-T7	GTAATACGACTCACTATAGGGAGACCACATTATGTATGTCTACGCCGC	
vir-F-T3	TGTTGGGAAATCACTCCCAATTAACGAAATGTCGTACAAGGTGC	530
vir-R-T7	GTAATACGACTCACTATAGGGAGACCACGATCTCCGGGAAAAGTGGTT	
nito-F-T3	TGTTGGGAAATCACTCCCAATTAACTCCGATTGATCCCTACGAT	1324
nito-R-T7	GTAATACGACTCACTATAGGGAGACCACGTATCTCCGTCCGTCAAATG	
Ythdc1-F-T3	TGTTGGGAAATCACTCCCAATTAACGAATCGAATGGTGGAGACT	622
Ythdc1-R-T7	GTAATACGACTCACTATAGGGAGACCACCCGTGTGTCTCGGAATAGGT	

E

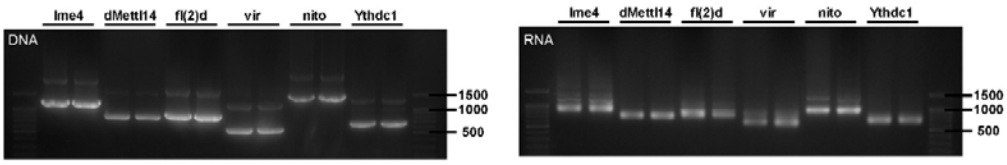

1326

1327 **Figure 1—figure supplement 1.** Primers of m^{6}A methyltransferases and reader protein for

1328 RT-qPCR and TSA-FISH. (**A**) The sequences of RT-qPCR primers. (**B**) Agarose gel electrophoresis

validation of qPCR primers. The left lane of each gene is negative control with primers only and no DNA substrate. (**C**) RT-qPCR analysis of mRNA levels of m^6A methyltransferases and reader protein in the brains of wildtype and trisomy *Drosophila* larvae. CF, wildtype female control; CM, wildtype male control; 2LF, trisomy 2L female; 2LM, trisomy 2L male; XXX, metafemale. Student's *t* test *p < 0.05, **p < 0.01, ***p < 0.001. (**D**) The sequences of FISH primers. (**E**) The sizes of the products of the FISH primers after PCR amplification and in vitro transcription were tested by agarose gel electrophoresis. 2L, chromosome 2 left arm; RT-qPCR, Real-time quantitative PCR; TSA-FISH, Tyramide signal amplification-based fluorescence *in situ* hybridization.

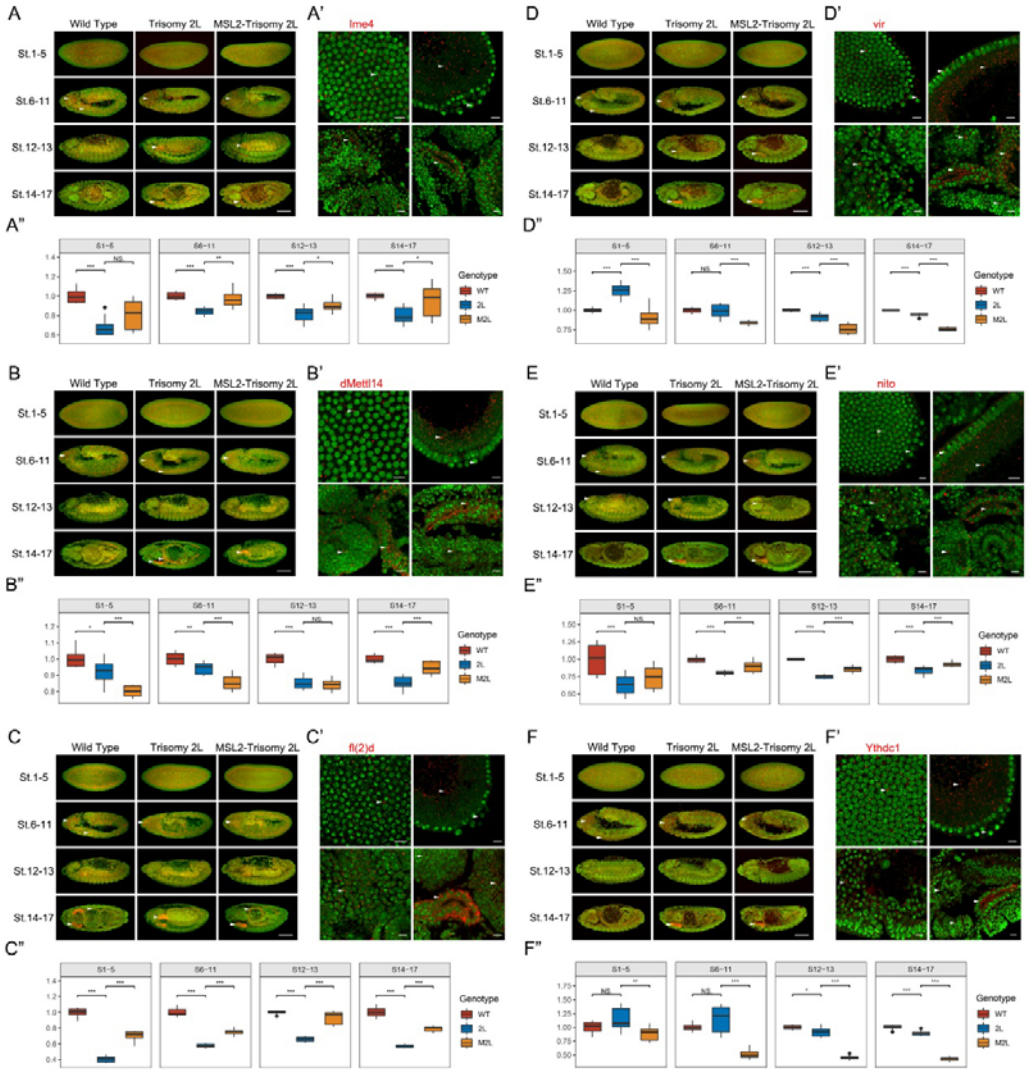

Figure 1—figure supplement 2. Embryo TSA-FISH of m^6A components in wildtype, trisomy, and MSL2-overexpressed trisomy *Drosophila*. The images represent m^6A component *Ime4* (**A-A"**),

1341 *dMettl14* (**B-B”**), *fl(2)d* (**C-C”**), *vir* (**D-D”**), *nito* (**E-E”**), and *Ythdc1* (**F-F”**), respectively. (**A-F**) Gene
1342 expression patterns in entire embryos. The genotypes of the samples were shown above, and the
1343 development stages (St.) were shown in the left of the pictures. The red pseudocolor represents
1344 signal from the probes, and green is the signal of nucleus. Arrowheads indicate regions where the
1345 probe signal are enriched. Scale bars, 100 µm. (**A’-F’**) RNA subcellular location patterns of m^6A
1346 components. Arrowheads indicate probe signals. Scale bars, 10 µm. (**A”-F”**) The expression levels
1347 of m^6A component genes represented as relative fluorescence intensity of the probes compared
1348 with DAPI. The expression of wildtype embryos was set as base line. WT, wildtype; 2L, trisomy 2L;
1349 M2L, MSL2-overexpressed trisomy 2L. Sample size = 10. Student’s *t* test *p < 0.05, **p < 0.01,
1350 ***p < 0.001.
1351

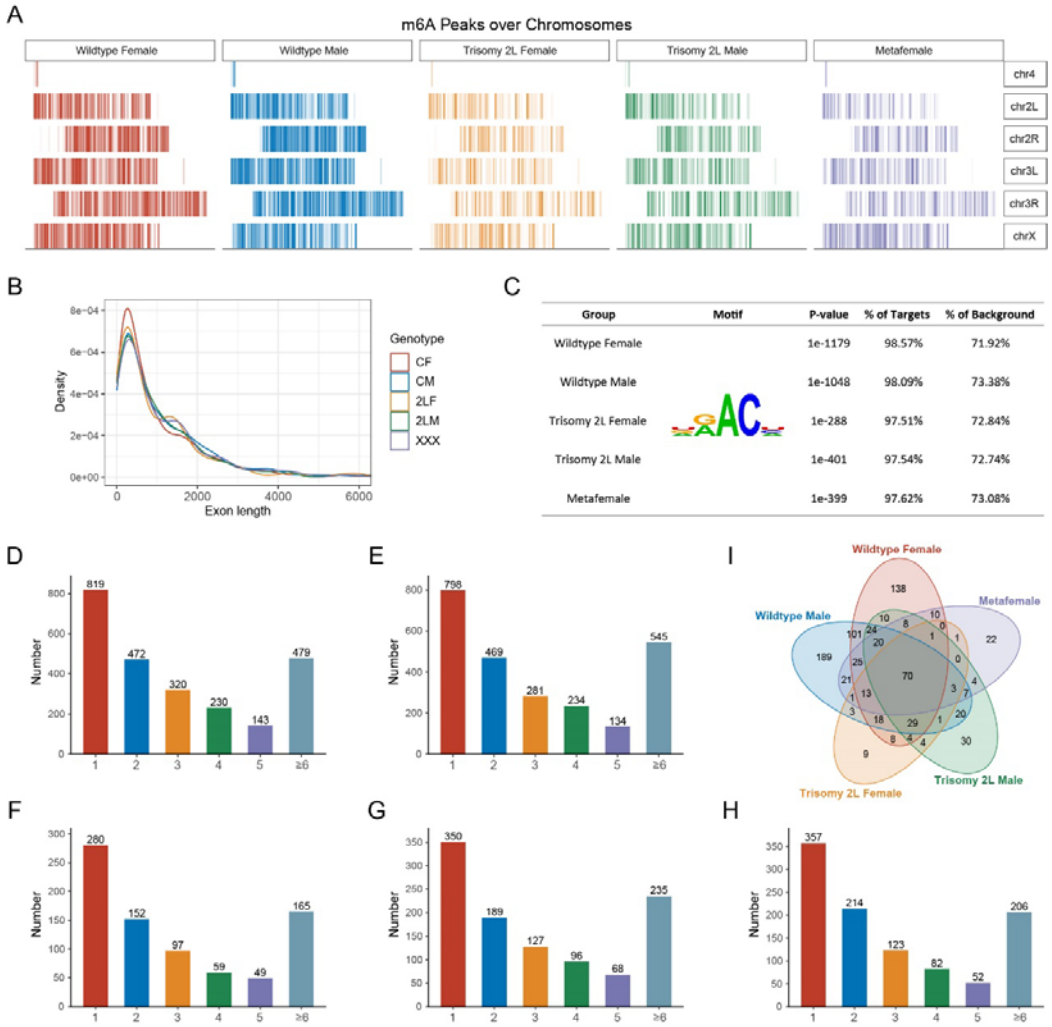

1352

1353 **Figure 2—figure supplement 1.** Characteristics of m^6A-modified genes in wildtype and aneuploid

Drosophila. (**A**) Distribution of m^{6}A peaks along each chromosome. (**B**) Kernel density plot showing the distribution of exon lengths of m^{6}A-modified genes. CF, wildtype female control; CM, wildtype male control; 2LF, trisomy 2L female; 2LM, trisomy 2L male; XXX, metafemale. (**C**) Enrichment analysis performed on the known m^{6}A consensus motif DRACH (D = G/A/U, R = G/A, H = U/A/C). (**D-H**) Statistics of the number of m^{6}A peaks on m^{6}A-modified genes in wildtype females (**D**), wildtype males (**E**), trisomy 2L females (**F**), trisomy 2L males (**G**), and metafemales (**H**). (**I**) Venn diagram showing the number of m^{6}A-modified genes with more than five m^{6}A peaks.

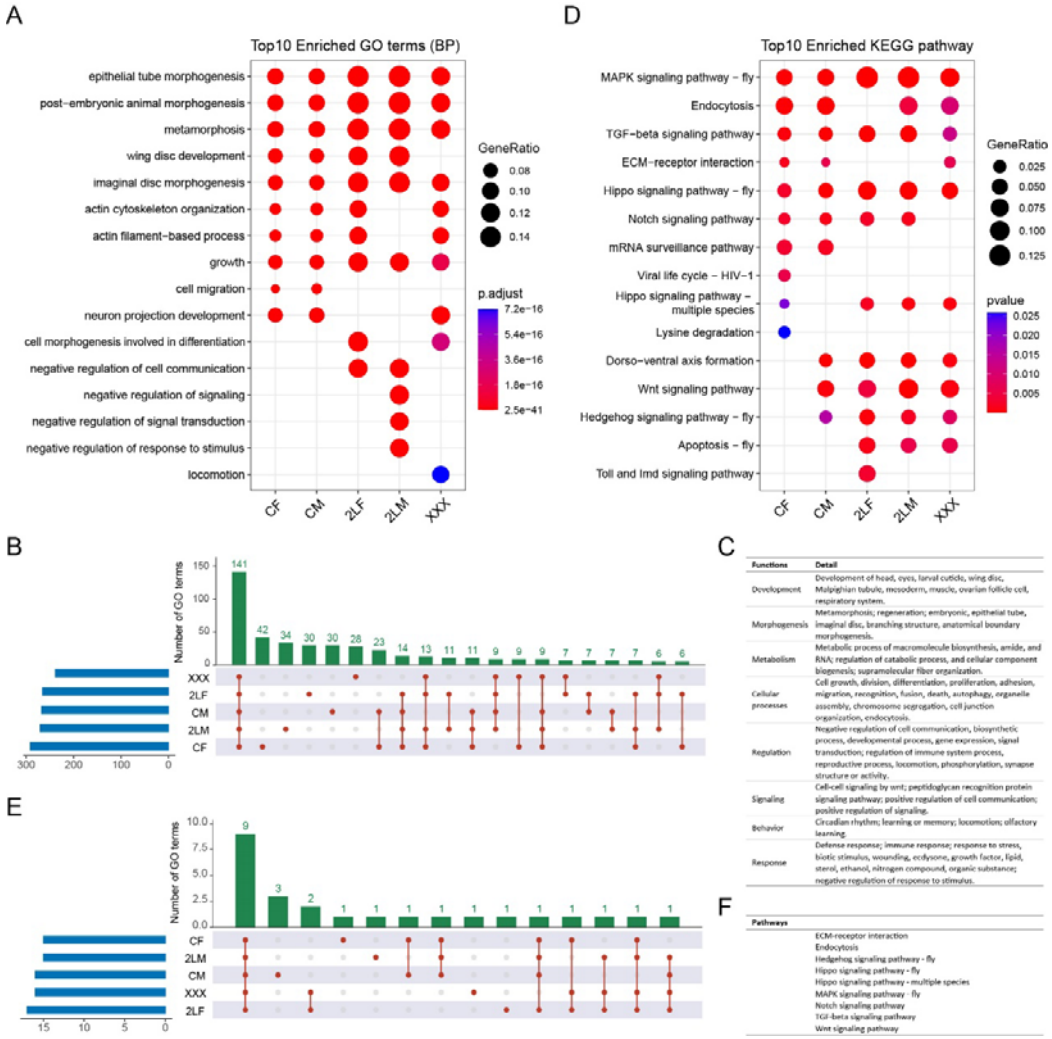

Figure 2—figure supplement 2. Functional and pathway analysis of m^{6}A-modified genes in wildtype and aneuploid *Drosophila*. (**A**) Functional enrichment analysis of m^{6}A-modified genes. Top 10 enriched GO terms (Biological Process) with adjusted p-value < 0.05 in each sample were

1367 shown. (**B**) UpSet plot showing the shared sets of enriched GO terms of m^6A-modified genes in
1368 different groups. (**C**) Summary of the common functions enriched by m^6A-modified genes in all
1369 genotypes. (**D**) KEGG pathway enrichment analysis of m^6A-modified genes. Top 10 enriched
1370 pathways with p-value < 0.05 in each sample were shown. (**E**) UpSet plot showing the shared sets
1371 of enriched KEGG pathways of m^6A-modified genes in different groups. (**F**) The pathways
1372 enriched in all genotypes were listed. CF, wildtype female control; CM, wildtype male control; 2LF,
1373 trisomy 2L female; 2LM, trisomy 2L male; XXX, metafemale; GO, Gene Ontology; BP, Biological
1374 Process; KEGG, Kyoto Encyclopedia of Genes and Genomes.
1375

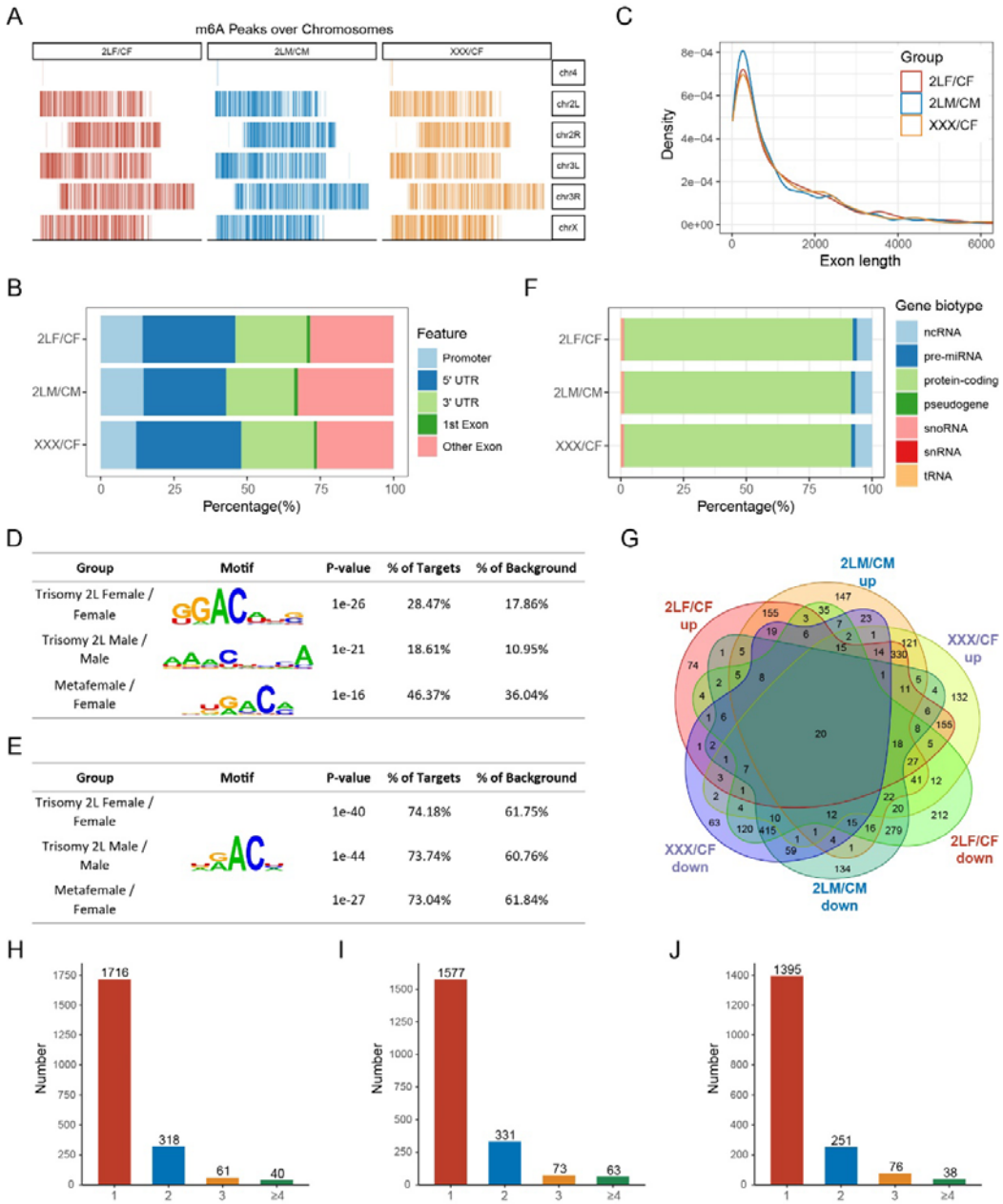

Figure 3—figure supplement 1. Characteristics of differentially methylated peak (DMP) associated genes. (**A**) Distribution of differentially methylated peaks (DMPs) along each chromosome. (**B**) Percentages of DMPs localized on different gene features. (**C**) Kernel density plot showing the distribution of exon lengths of DMP-associated genes. (**D**) The top enriched motifs with *de novo* motif analysis of DMPs in each comparison. (**E**) Enrichment analysis performed on the known m^6A consensus motif DRACH (D = G/A/U, R = G/A, H = U/A/C). (**F**) Gene biotypes of DMP-associated genes. (**G**) Venn diagram showing the intersection of DMP-associated genes in each comparison. (**H-J**) Statistics of the number of DMPs on DMP-associated genes in

trisomy 2L females compared with wildtype females (**H**), trisomy 2L males compared with wildtype males (**I**), and metafemales compared with wildtype females (**J**). CF, wildtype female control; CM, wildtype male control; 2LF, trisomy 2L female; 2LM, trisomy 2L male; XXX, metafemale; 5′UTR, 5′ untranslated region; 3′UTR, 3′ untranslated region.

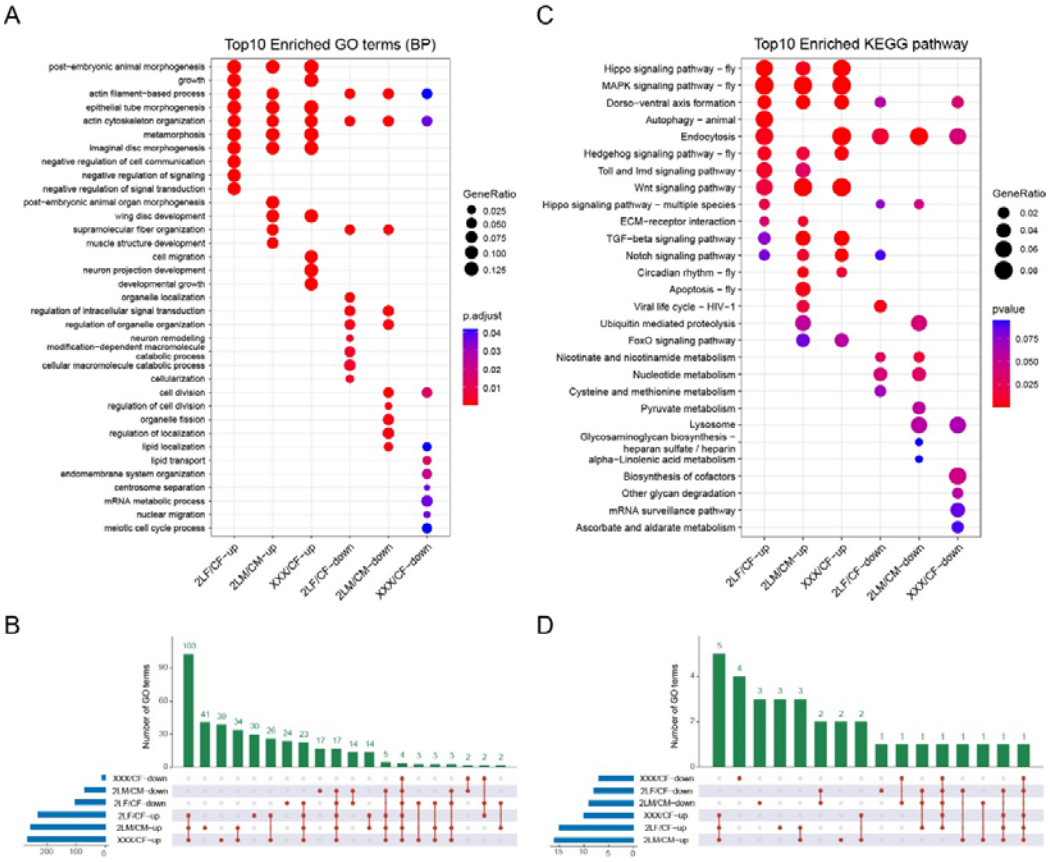

Figure 4—figure supplement 1. Functional and pathway analysis of DMP-associated genes. (**A**) Functional enrichment analysis of DMP-associated genes. Top 10 enriched GO terms (Biological Process) with adjusted p-value < 0.05 in each comparison were shown. (**B**) UpSet plot showing the shared sets of enriched GO terms of DMP-associated genes in different aneuploidies. (**C**) KEGG pathway enrichment analysis of DMP-associated genes. Top 10 enriched pathways with p-value < 0.1 in each comparison were shown. (**D**) UpSet plot showing the shared sets of enriched KEGG pathways of DMP-associated genes in different aneuploidies. CF, wildtype female control; CM, wildtype male control; 2LF, trisomy 2L female; 2LM, trisomy 2L male; XXX, metafemale.

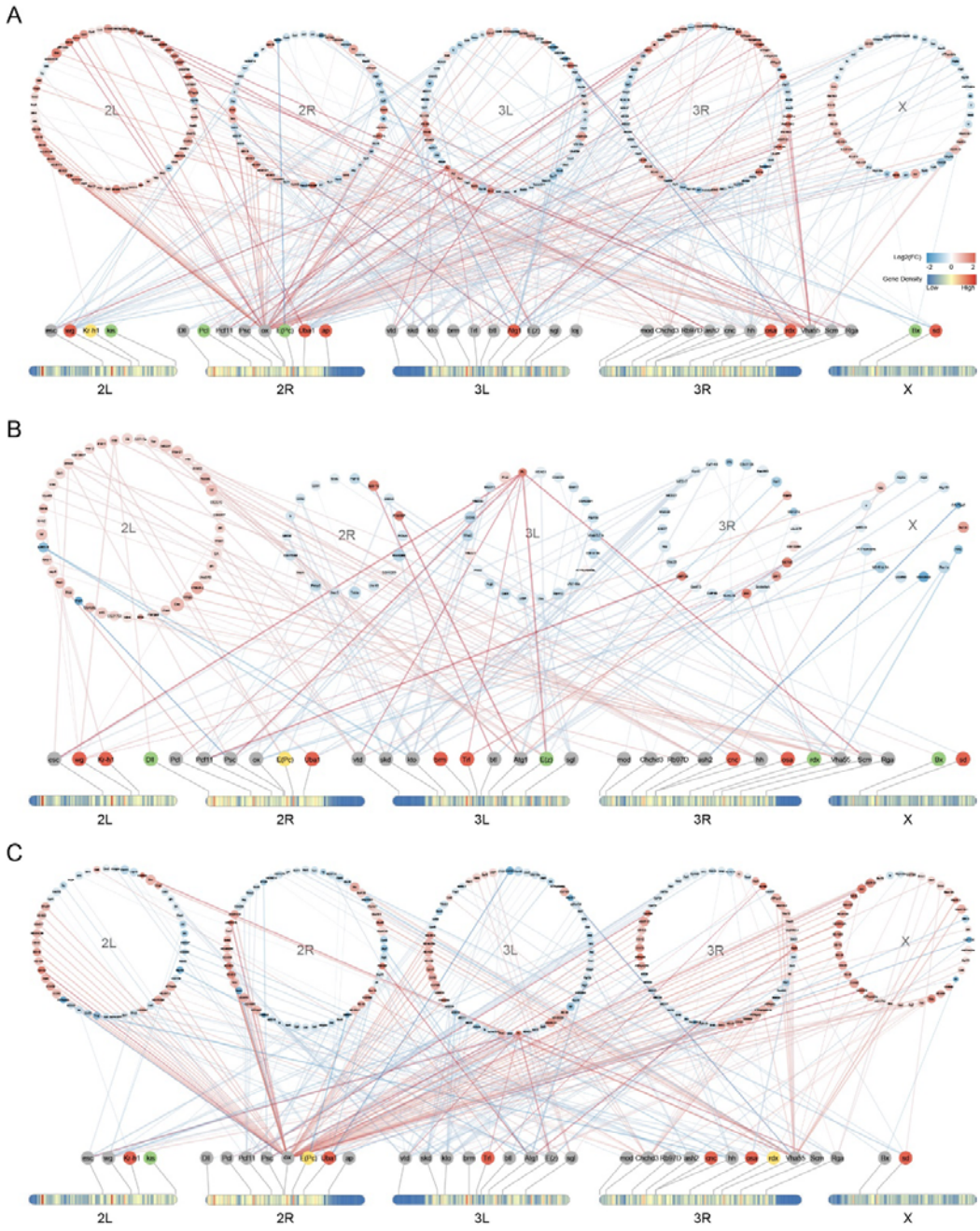

Figure 5—figure supplement 1. Dosage-sensitive modifiers and their interactors in aneuploid *Drosophila*. (**A**-**C**) Networks showing the methylation status of known dosage-sensitive modifiers and the expression changes of genes interact with these modifiers in trisomy 2L females (**A**), trisomy 2L males (**B**), and metafemales (**C**), respectively. Protein-protein interaction (PPI) relationships were obtained from the STRING database. The colors of the heatmaps on chromosomes represent the gene density. Dosage-sensitive modifiers were arranged according to their localizations, with red indicating genes with upregulated DMPs, green indicating genes with

1409 downregulated DMPs, yellow indicating genes with both up- and down-regulated DMPs, and grey
1410 indicating genes without DMPs. The interactors of these modifiers were also separated by
1411 chromosomes, and the colors of the nodes and edges indicate the log2(fold changes) of gene
1412 expression in trisomies. The width of the edges represents the combined score, and only
1413 interactions with combined score ≥ 700 were selected for presentation.
1414

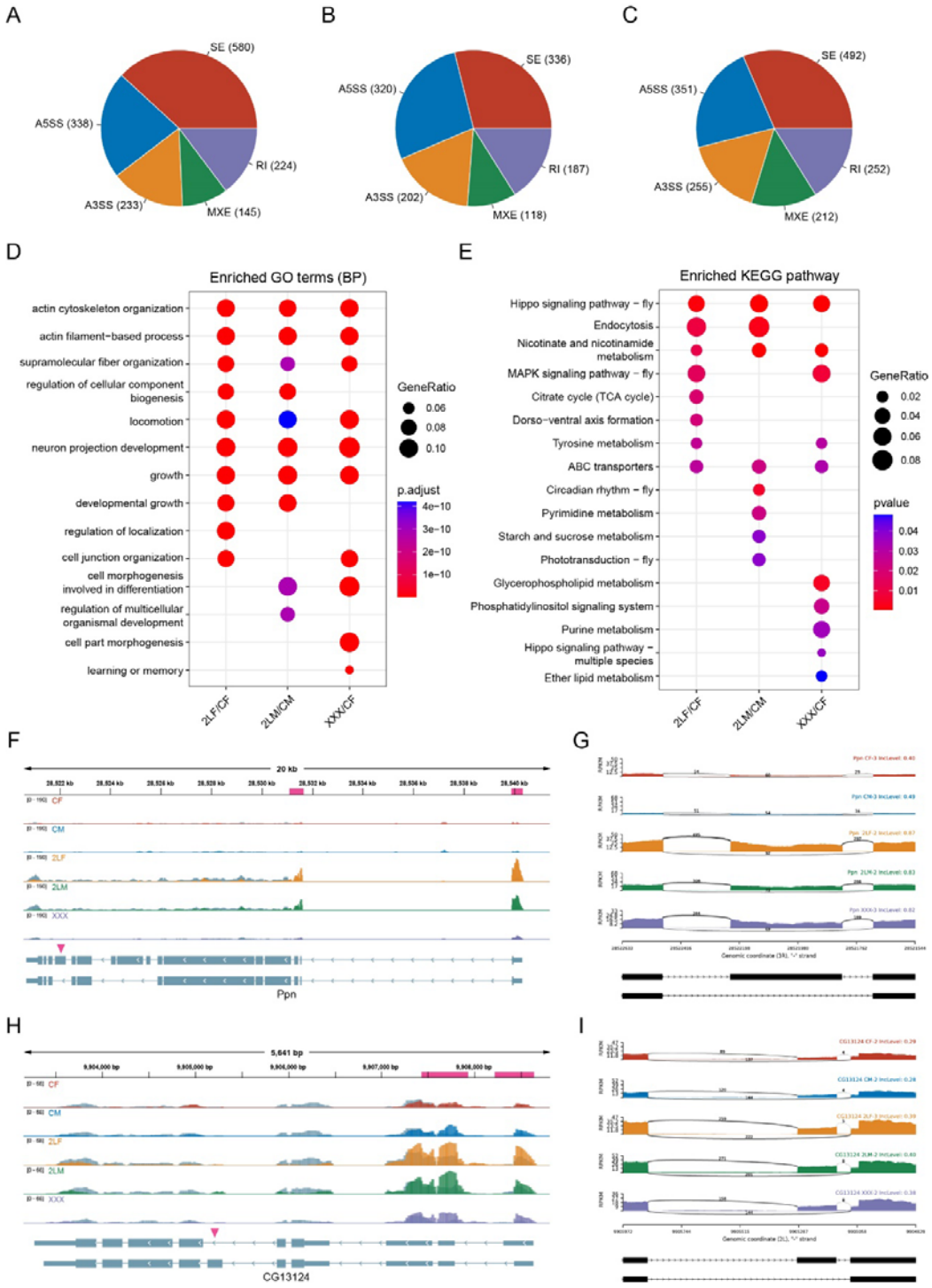

Figure 6—figure supplement 1. Alternative splicing analysis in aneuploidies. (**A-C**) Numbers of differential alternative splicing events in trisomy 2L females (**A**), trisomy 2L males (**B**), and metafemales (**C**). SE, skipped exon; A5SS, alternative 5′ splice site; A3SS, alternative 3′ splice site; MXE, mutually exclusive exons; RI, retained intron. (**D**) Functional enrichment analysis of differentially alternatively spliced genes. Top 10 enriched GO terms (Biological Process) with

1421 p-value < 0.05 in each comparison were shown. (**E**) KEGG pathway enrichment analysis of
1422 differentially alternatively spliced genes. Top 10 enriched pathways with p-value < 0.05 in each
1423 comparison were shown. (**F**,**H**) Genome browser example of *Ppn* (**F**) and *CG13124* (**H**) for
1424 indicated MeRIP-seq data. Steelblue color represents input reads, while other colors represent IP
1425 reads. Signals were displayed as the mean CPM of two biological replicates. The gene
1426 architectures were shown at the bottom (only two representative transcript isoforms were
1427 shown). The magenta rectangles at above represent DMPs. The magenta arrowheads indicate the
1428 positions of differential alternative splicing. (**G**,**I**) Sashimi plots depicting RNA sequencing reads
1429 and exon junction reads at the positions where the differential splicing events occurs on *Ppn* (**G**)
1430 and *CG13124* (**I**). The gene models were shown below. One of the biological replicates was
1431 chosen for representation. CF, wildtype female control; CM, wildtype male control; 2LF, trisomy
1432 2L female; 2LM, trisomy 2L male; XXX, metafemale; CPM, Counts per million; RPKM, Reads per
1433 kilobase per million mapped reads.
1434
1435

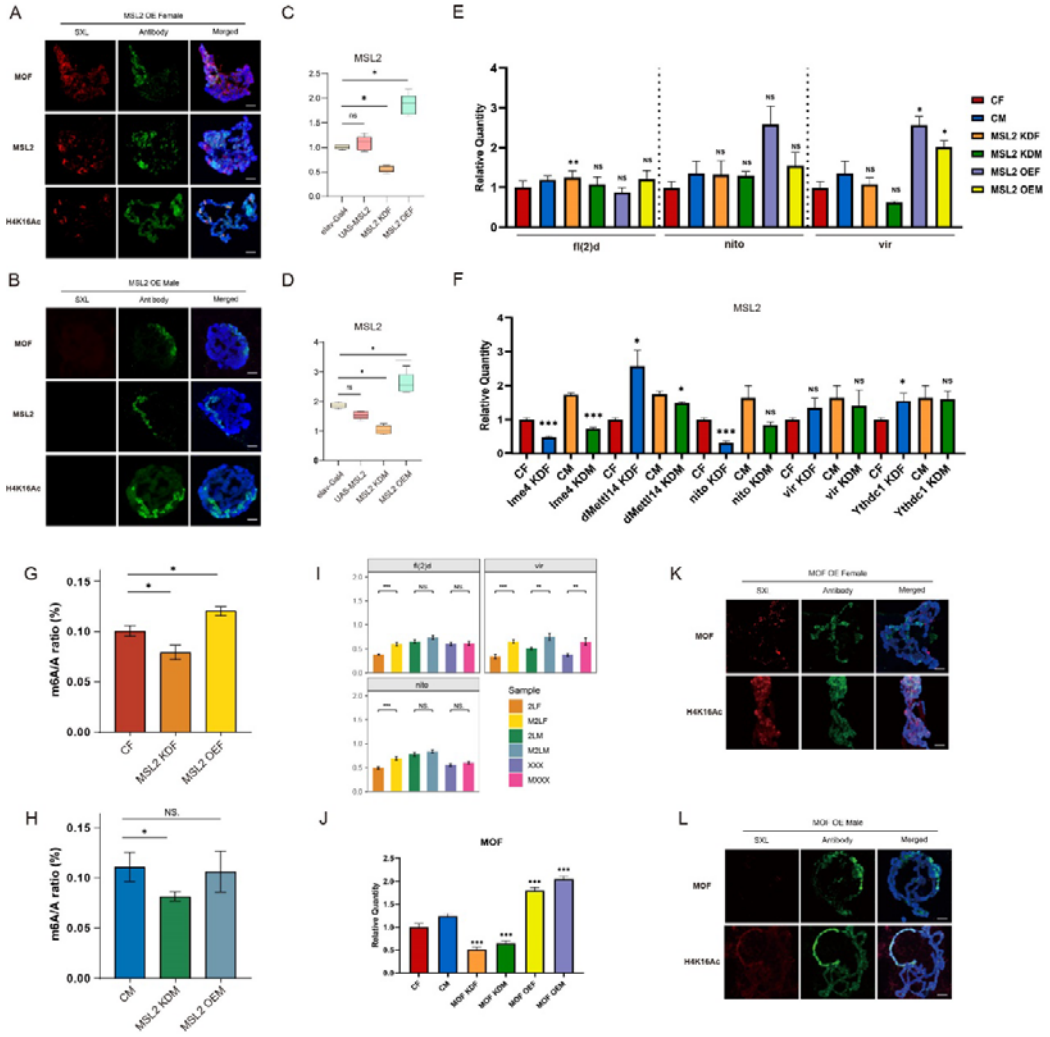

Figure 7—figure supplement 1. The relationships between m^{6}A methylation and MSL complex. (**A**,**C**) Immunofluorescence of polytene chromosomes in MSL2-overexpressed female (**A**) and male (**C**) larvae. The red channel is the signal from SXL and the green channel is the signal from antibodies of MSL complex components. DNA is stained with DAPI in blue. Scale bars, 10 µm. OE, overexpressed. (**B**,**D**) RT-qPCR analysis of mRNA levels of MSL2 in the heads of MSL2 transgenic female (**B**) and male (**D**) *Drosophila* adults. Student's *t* test *p < 0.05, **p < 0.01, ***p < 0.001. OE, overexpressed. (**E**) RT-qPCR analysis of mRNA levels of m^{6}A regulators in the heads of MSL2 transgenic *Drosophila*. Student's *t* test *p < 0.05, **p < 0.01, ***p < 0.001. CF, wildtype female control; CM, wildtype male control; OEF, overexpressed female; OEM, overexpressed male; KDF, knockdown female; KDM, knockdown male. (**F**) RT-qPCR analysis of mRNA levels of MSL2 in the heads of m^{6}A regulators knockdown *Drosophila*. Student's *t* test *p < 0.05, **p < 0.01, ***p < 0.001. CF, wildtype female control; CM, wildtype male control; OEF, overexpressed female; OEM,

1449 overexpressed male; KDF, knockdown female; KDM, knockdown male. (**G**,**H**) Abundance of total
1450 RNA m^6A modification in the heads of MSL2 transgenic females (**G**) and males (**H**). Student's *t* test
1451 *p < 0.05, **p < 0.01, ***p < 0.001. MSL2 KDF, MSL2 neural-knockdown female; MSL2 KDM,
1452 MSL2 neural-knockdown male; MSL2 OEF, MSL2-overexpressed female; MSL2 OEM,
1453 MSL2-overexpressed male. (**I**) RT-qPCR analysis of mRNA levels of m^6A regulators in the brains of
1454 trisomy and MSL2-overexpressed trisomy *Drosophila* larvae. Student's *t* test *p < 0.05, **p < 0.01,
1455 ***p < 0.001. 2LF, trisomy 2L female; 2LM, trisomy 2L male; XXX, metafemale; M2LF,
1456 MSL2-overexpressed trisomy 2L female; M2LM, MSL2-overexpressed trisomy 2L male; MXXX,
1457 MSL2-overexpressed metafemale. (**J**) RT-qPCR analysis of mRNA levels of MOF in the heads of
1458 MOF transgenic *Drosophila*. Student's t test *p < 0.05, **p < 0.01, ***p < 0.001. CF, wildtype
1459 female control; CM, wildtype male control; OEF, overexpressed female; OEM, overexpressed male;
1460 KDF, knockdown female; KDM, knockdown male. (**K,L**) Immunofluorescence of polytene
1461 chromosomes in MOF-overexpressed female (**H**) and male (**I**) larvae. The red channel is the signal
1462 from SXL and the green channel is the signal from MOF or H4K16Ac. DNA is stained with DAPI in
1463 blue. Scale bars, 10 µm. OE, overexpressed.
1464

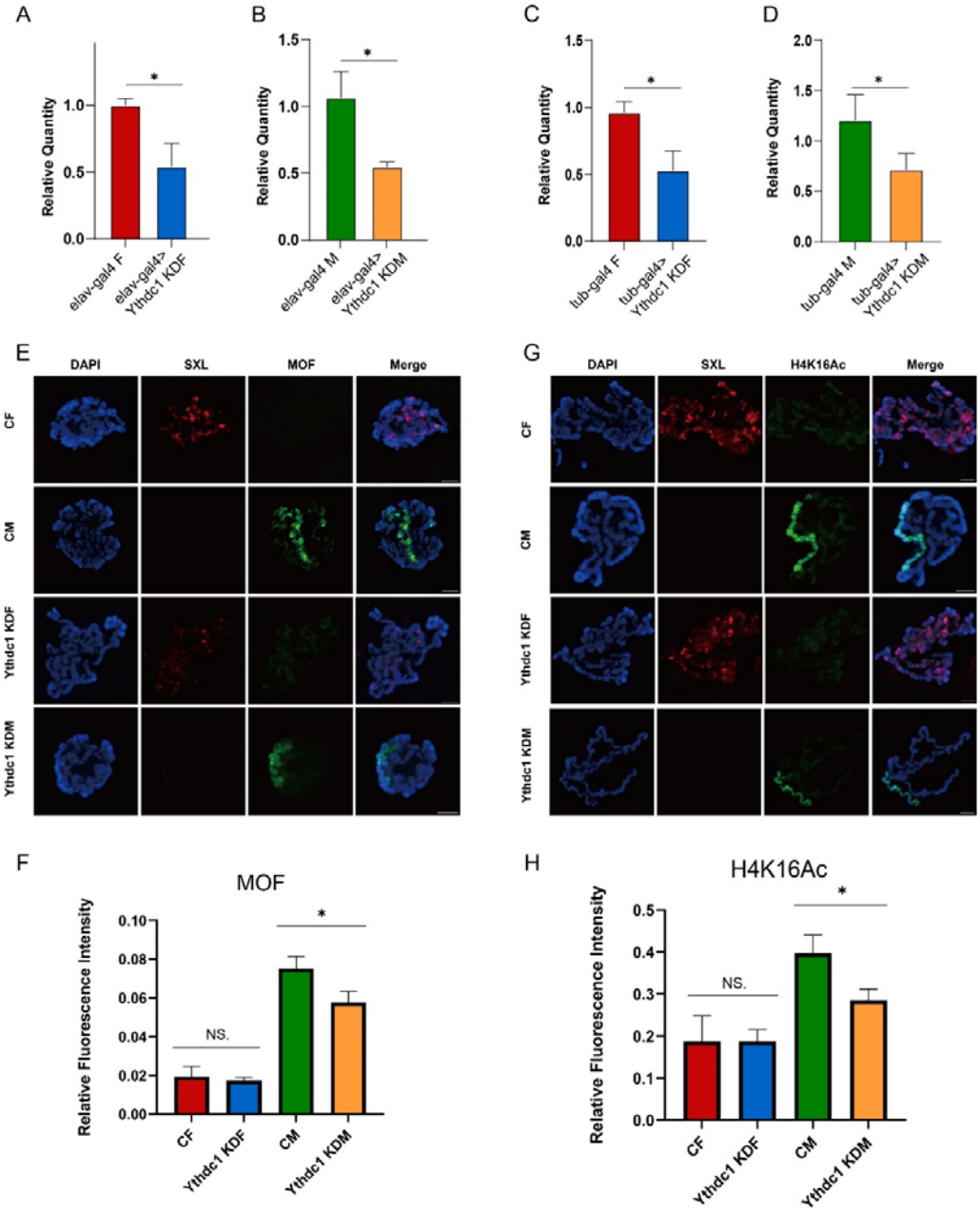

Figure 8—figure supplement 1. Ythdc1 may regulate H4K16Ac through histone acetyltransferase MOF. (**A**,**B**) RT-qPCR analysis of mRNA levels of Ythdc1 in the heads of *Ythdc1* neural-knockdown female (**A**) and male (**B**). elav-gal4>Ythdc1 KDF, Ythdc1 neural-knockdown female; elav-gal4>Ythdc1 KDM, Ythdc1 neural-knockdown male. (**C**,**D**) RT-qPCR analysis of mRNA levels of Ythdc1 in *Ythdc1* knockdown female (**C**) and male (**D**) adult *Drosophila*. tub-gal4>Ythdc1 KDF, Ythdc1 knockdown female; tub-gal4>Ythdc1 KDM, Ythdc1 knockdown male. (**E**) Immunofluorescence of polytene chromosomes showed the signals of SXL (red channel) and MOF (green channel) in the salivary glands of *Drosophila* larvae of different genotypes. (**F**) The

1474 levels of MOF in the salivary glands of Ythdc1 knockdown *Drosophila* quantified by
1475 immunofluorescence. (**G**) Immunofluorescence of polytene chromosomes showed the signals of
1476 SXL (red channel) and H4K16Ac (green channel) in the salivary glands of *Drosophila* larvae of
1477 different genotypes. (**H**) The levels of H4K16Ac in the salivary glands of Ythdc1 knockdown
1478 *Drosophila* quantified by immunofluorescence. Ythdc1 KDF, Ythdc1 knockdown female; Ythdc1
1479 KDM, Ythdc1 knockdown male. Scale bars, 10 µm. Student's *t* test *p < 0.05, **p < 0.01, ***p <
1480 0.001.

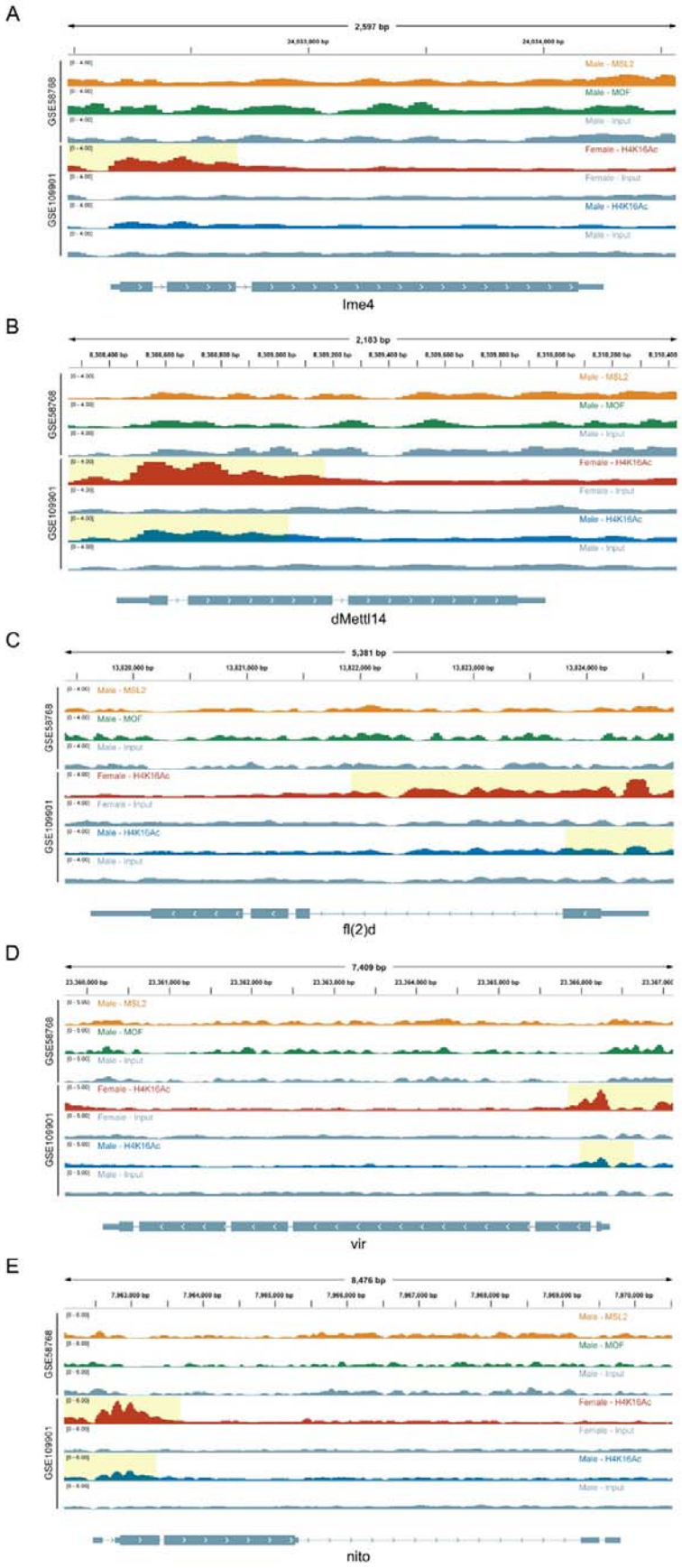
A
2,597 bp
GSE58768
GSE109901
Male - MSL2
Male - MOF
Male - Input
Female - H4K16Ac
Female - Input
Male - H4K16Ac
Male - Input
Ime4
B
2,183 bp
GSE58768
GSE109901
Male - MSL2
Male - MOF
Male - Input
Female - H4K16Ac
Female - Input
Male - H4K16Ac
Male - Input
dMettl14
C
5,281 bp
GSE58768
GSE109901
Male - MSL2
Male - MOF
Male - Input
Female - H4K16Ac
Female - Input
Male - H4K16Ac
Male - Input
fl(2)d
D
7,409 bp
GSE58768
GSE109901
Male - MSL2
Male - MOF
Male - Input
Female - H4K16Ac
Female - Input
Male - H4K16Ac
Male - Input
vir
E
8,476 bp
GSE58768
GSE109901
Male - MSL2
Male - MOF
Male - Input
Female - H4K16Ac
Female - Input
Male - H4K16Ac
Male - Input
nito

1481

1482 **Figure 8—figure supplement 2.** Genome browser example of m^6A regulator genes for indicated
1483 ChIP-seq data. H4K16Ac, MSL2, and MOF ChIP-seq results for gene *Ime4* (**A**), *dMettl14* (**B**), *fl(2)d*
1484 (**C**), *vir* (**D**), and *nito* (**E**) are shown, respectively. Signals were displayed as CPM values. The gene
1485 architectures were shown at the bottom (only one representative transcript isoform was shown).
1486 The yellow shaded area indicates the presence of the H4K16Ac peaks.
1487
1488